We are IntechOpen,
the world's leading publisher of
Open Access books
Built by scientists, for scientists

6,900
Open access books available

186,000
International authors and editors

200M
Downloads

Our authors are among the

154
Countries delivered to

TOP 1%
most cited scientists

12.2%
Contributors from top 500 universities

CLARIVATE ANALYTICS
BOOK CITATION INDEX
INDEXED

WEB OF SCIENCE™

Selection of our books indexed in the Book Citation Index
in Web of Science™ Core Collection (BKCI)

Interested in publishing with us?
Contact book.department@intechopen.com

Numbers displayed above are based on latest data collected.
For more information visit www.intechopen.com

Simulation Methods for the Transient Analysis of Synchronous Alternators

Jérôme Cros, Stéphanie Rakotovololona, Maxim Bergeron, Jessy Mathault, Bouali Rouached, Mathieu Kirouac and Philippe Viarouge

Additional information is available at the end of the chapter

Abstract

The integration of unconventional renewable energy sources on the electrical grid poses challenges to the electrical engineer. This chapter focuses on the transient modeling of electrical machines. These models can be used for the design of generator control, the definition of the protection strategies, stability studies, and the evaluation of the electrical; mechanical; and thermal constraints on the machine. This chapter presents three modeling techniques: the standard d-q equivalent model, the coupled-circuit model, and the finite element model (FEM). The consideration of magnetic saturation for the different models is presented. The responses of the different models during three-phase, two-phase, and one-phase sudden short circuit are compared.

Keywords: Power generator, Synchronous alternator, electrical machine modeling, dq model, coupled circuits, finite element analysis

1. Introduction

There are mainly two types of large synchronous alternators having a wound rotor: the round rotor and the salient pole rotor [1]. Generally, these synchronous alternators are directly connected to the grid in parallel, with many other alternators. In this case, the stator voltage and the frequency (f) are imposed by the grid and the generators work at a fixed speed (n) depending on the number of magnetic pole pairs in the machine (p); ($n = 60 \cdot f / p$). For example, a round rotor synchronous generator with $p=1$ would have a speed of $n=3600$ rpm on an $f=60$ Hz electrical grid. Synchronous generators with $p=1, 2$ are known

as turbo generators and present a round-shaped rotor. The prime mover of large turbo generators are generally steam turbines, which operate at high speeds. In other cases, the prime mover runs at low speeds, so that salient pole synchronous generators are used. The largest salient pole generators are used in dams for the production of electricity with hydraulic turbine. The optimal speed of a hydraulic turbine is relatively slow; thus, the generator has a high number of poles.

The growing demand for energy and care for environment protection is spurring the development and integration of unconventional renewable energy sources such as solar, wind, and tidal power. The unconventional renewable energy brings challenges on the generator design as the energy production cannot always be done at fixed prime mover speed. In this case, different kinds of generators can be used, and generally, they are associated with power electronic converters to connect to the grid. For example, the main type of generators used for speed-varying applications is the doubly fed induction generators (DFIG) [2-3]. The stator winding of these machines is directly connected to the grid, but there is a three-phase winding on the rotor that is fed through power electronics. Such machine designs can create a rotating field, going faster, slower, or at the constant speed than the rotor. Thus, the stator frequency can be imposed regardless of the rotor speed. For a given generator, the larger the speed deviation is allowed, the larger the rating of the power electronics must be in order to deliver the rated power. Conventional synchronous generators are also used for variable speed applications by using a power electronic converter connected to the stator winding.

The integration of unconventional renewable energy must not be made at the cost of a less reliable power distribution. A reliable power distribution network is characterized by a robust design of its equipment, control, and protection strategies [4-5]. The voltage and power distribution on the grid is maintained mostly by the proper control of torque and excitation of the generators. Accurate steady-state and transient models of the electrical machine are required [4-6].

Modeling a generator is a real challenge, as an accurate representation of the machine must deal with many internal considerations, such as the saturation effects, nonlinearity of the material's properties, rotational effects, and the large number of complex current paths inside the generator. Such a detailed analysis provides information on the stator voltage harmonics, copper/iron losses, and torque ripples. This detailed analysis is of high importance for the reliable design at all operating points. However, the performance of a model in terms of accuracy and computational effort depend on its simplifying assumptions.

Transient machine models can be divided into three types: phase-domain model, d-q model, and finite element model. The phase-domain model is an analytical approach based on the voltage and flux-current equations of the synchronous machine expressed in the fixed a-b-c reference frame [7-9]. It requires precise knowledge of the time-dependent inductance matrix, which can be a difficult task. Hence, many researchers use time-stepping finite element analysis to determine the unknown matrix for a certain discretization [9]. This approach is known as "coupled finite element state space approach."

The d-q model is also based on the voltage and flux-current equations but expressed in a virtual reference frame rotating at synchronous speed [7-8]. Based on certain assumptions, this model represents synchronous machines by two magnetically decoupled equivalent circuits comprising lumped *R-L* parameters. Many identification methods are found in the literature for the d-q model parameters, such as the *standstill time response* (SSTR) tests, the *rotating time-domain response* (RTDR) tests, the *standstill frequency response* (SSFR) tests [10], the *open-circuit frequency response* (OCFR) tests, and the *on-line frequency response* (OLFR) tests. More recent approaches include *online measurements* techniques. These methods are well reviewed in the literature [11].

Finally, the finite element model is used in solving numerically the general equations of electromagnetics [12]. It is the most accurate of the three types, but also the most expensive in terms of computational effort. Nonlinear phenomena such as saturation and skin effects can be taken into account by this model.

In this chapter, the three types of transient electrical machine models are presented and compared. Understanding these differences, identification methods, and scope of these models provide useful information to the electrical engineer to determine the problems that can be treated with each model. The chapter is divided into following sections:

• Presentation of the generator used for experiments and model validations

• The standard d-q equivalent model and the SSFR-identification method

• The detailed coupled-circuit model

• The finite element model

• Improvements to the models in order to consider the saturation

• Comparison of the models in order to simulate different kind of short circuits

2. Synchronous generator used for this study

The machine used for the experiments is a three-phase 5.4-kVA round rotor synchronous generator. The stator has 54 slots. The rotor has three concentric coils per pole and a total of 24 copper damper bars connected by short-circuit rings (Figure 1).

The stator lamination stack is shown in Figure 2. The winding of this machine is of a special construction; it is made of rectangular conductors, and there are 14 conductors per slot distributed in four layers. They are soldered in the extremity in order to put the individual conductors in series to form coils. It can be seen that the stator slots are almost closed near the air gap (Figure 2). Data of the generator nameplate are given in Table 1. Figures 3 and 4 present, respectively, half of the rotor and stator laminations. The main dimensions are given in millimeter. Figure 5 presents the stator-winding repetitive section.
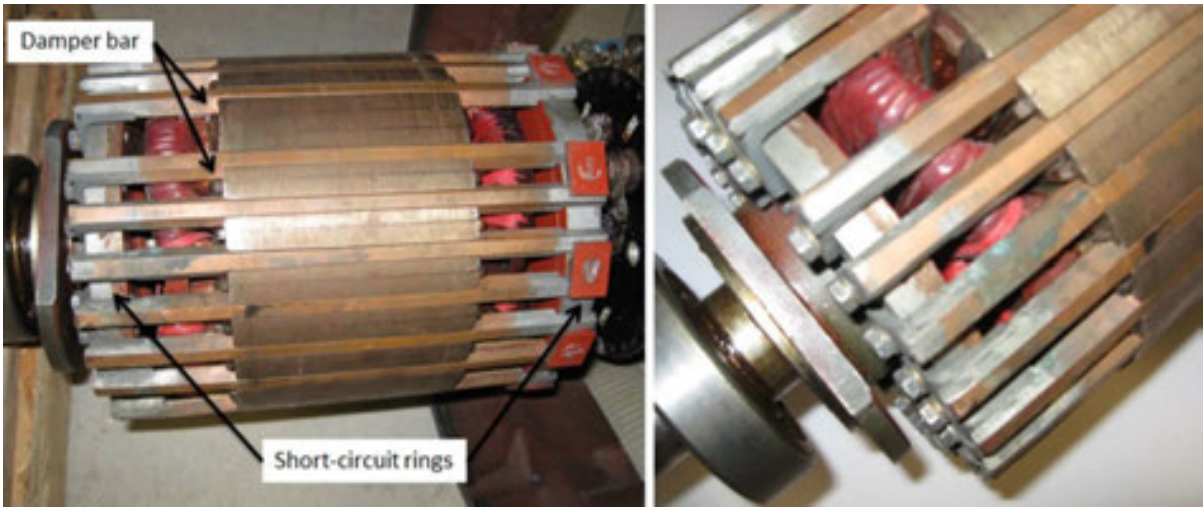
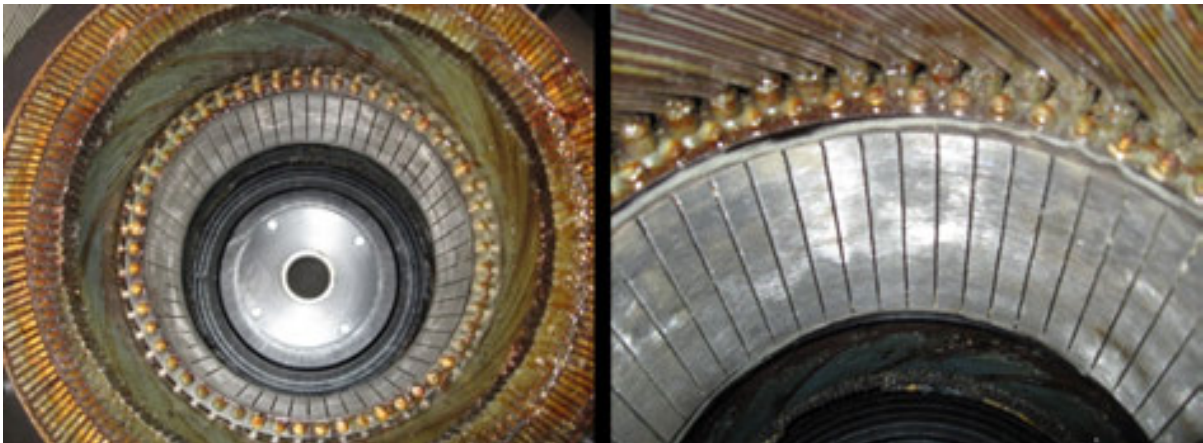**Figure 1.** Rotor of the synchronous generator

Figure 2. Stator on the side of end-winding connections

Power	5.4 kVA
Electrical frequency	60 Hz
Line-to-line voltage	280 V
Stator phase current (star connected)	11.1 A
Rotor field current for the nominal no-load voltage	0.5 A
Speed	1800 rpm

Table 1. Nominal parameters

Table 1: Nominal parameters

Power	5.4 kVA
Electrical frequency	60 Hz
Line-to-line voltage	280 V
Stator phase current (star connected)	11.1 A
Rotor field current for the nominal no-load voltage	0.5 A
Speed	1800 rpm

Table 2: Main parameters

Phase winding; number of turns: 156	Phase resistance: 0.156 Ω
Field winding; number of turns: 2208	Field resistance: 21.5 Ω
Damper bars resistivity: 22 nΩ.m	DC bar resistance: 21 μΩ
Contact ring resistance: 170 μΩ	End-field winding: 0.8 Hz
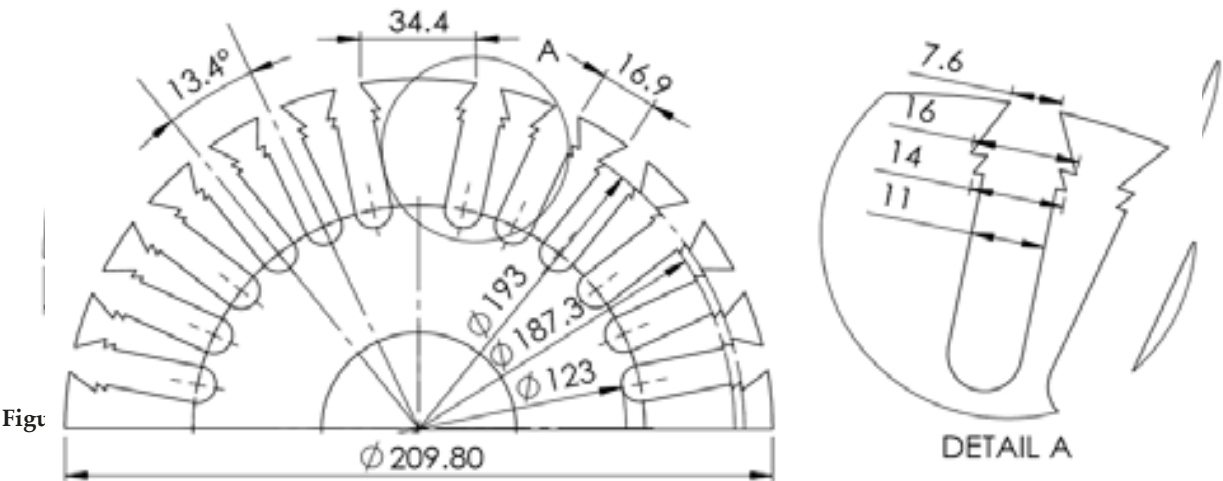
Figure 3: Rotor steel laminations

Stack length: 105mm
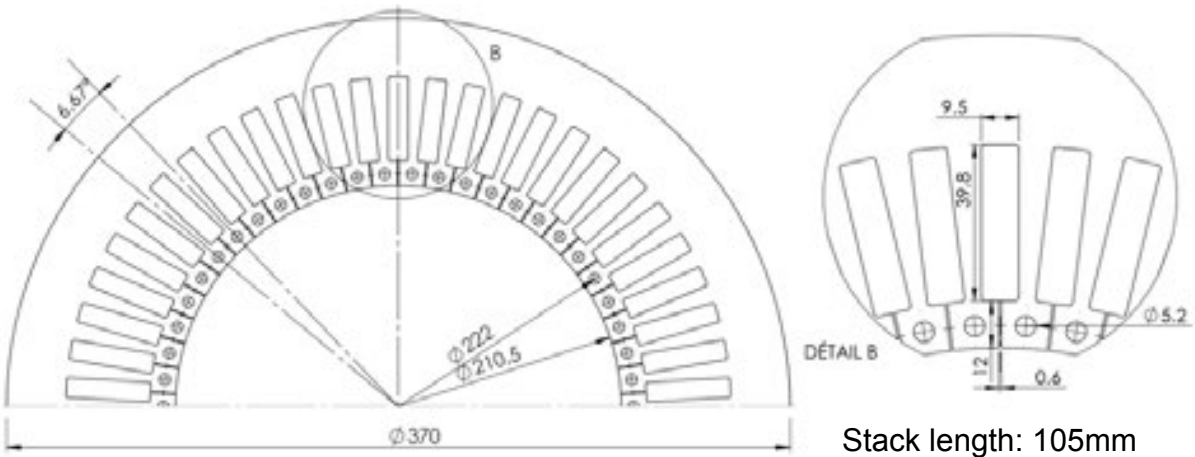
Figure 4: Stator steel laminations

Figure 4. Stator steel laminations

1	2	3	4	5	6	7	8	9	10	11	12	13	14	15	16	17	18	19	20	21	22	23	24	25	26	27
A1	A2	A3	A4	A	5	6	7	8	9	10	11	12	13	14	15	16	17	18	19	20	21	22	23	24	25	26	27
A	A	A	A	A	B'	B'	B'	B'	B'	B	B	C	C	C'	C'	C'	A''	A''	A'	A'	B	B	C	C	C	C	A
A	A	A	A	A	B'	B'	B'	B'	B'	B	B	C	C	C	C	A''	A''	A''	A'	A'	B	B	B	C'	C'	C'	C	A
A	A	A	A	A	B'	B'	B'	B'	B'	B	B	C	C	C	C	A''	A''	A'	A'	A'	B	B	C	C	C	C	A	C

| Pôle 1 | | | | | | | | | | | | Pôle 2 | | | | | | | | | | | | | | | A |

Pas de 1 à 13

Pitch from 1 to 13

Figure 5: Stator-winding repetitive section
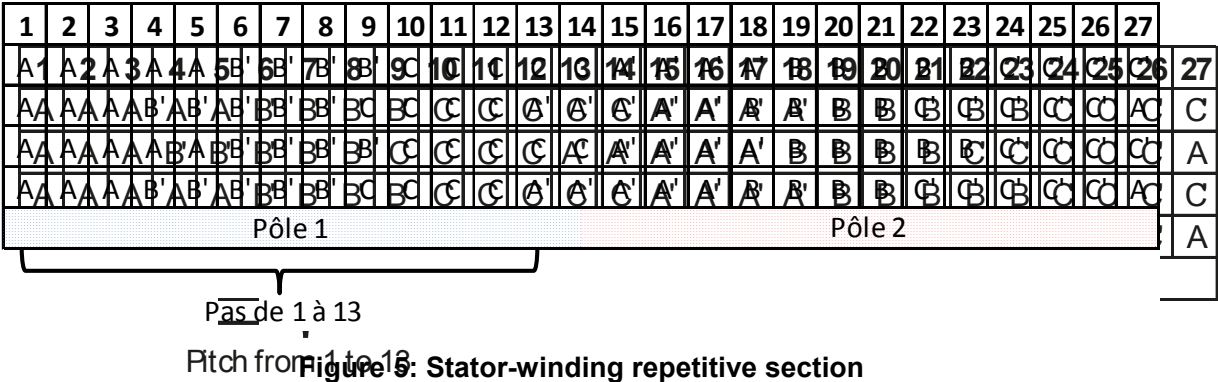
Figure 5. Stator-winding repetitive section

3. d-q equivalent model

3.1. Modeling method

The d-q model uses a transformation, known as the d-q transformation or Park transformation, in order to obtain a reference frame rotating with the rotor instead of the fixed stator frame [8]. The assumptions associated with the use of d-q transformation are presented below [7]:

- Magnetic saturation effects are neglected. By choosing two orthogonal axes, it is assumed that currents flowing in one axis do not produce flux in the other axis.
- The armature windings are sinusoidally distributed along the air gap so that each phase winding produces a sinusoidal magnetomotive force (mmf) wave. Hence, space harmonics are negligible and the induced voltage is purely sinusoidal.
- The stator slots do not cause appreciable variation of the rotor inductances with rotor position.
- Magnetic hysteresis is negligible.

Under these assumptions, synchronous machines are modeled by two independent, magnetically uncoupled circuits in d- and q-axes (Figure 6). Direct-axis model includes the d-axis armature winding, the field winding, and any additional equivalent damper windings. The damper bar elements (L_{nd}, R_{nd}) represent equivalent current paths in the d-axis damper bars or in the rotor steel body. The number of assumed rotor circuits determines the order of the model. The same approach applies to the q-axis network, except that the field winding is not present. The d-q model parameters are the R-L lumped circuit elements (Figure 6) as viewed from the stator. A detailed development of the d-q model is presented in [7].
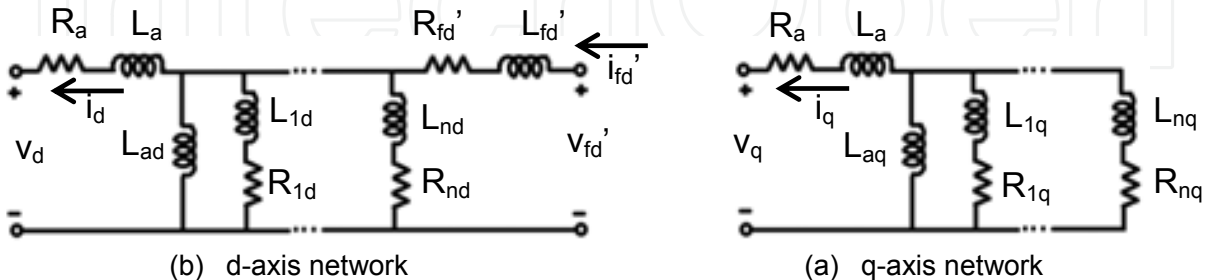
(b) d-axis network   (a) q-axis network

Figure 6: General d-q model equivalent circuit

Figure 6. General d-q model equivalent circuit

Under these assumptions, synchronous machines are modeled by two independent, magnetically uncoupled circuits in d- and q-axes (Figure 6). Direct-axis model includes the d-axis

armature winding, the field winding, and any additional equivalent damper windings. The damper bar elements (L_{nd}, R_{nd}) represent equivalent current paths in the d-axis damper bars or in the rotor steel body. The number of assumed rotor circuits determines the order of the model. The same approach applies to the q-axis network, except that the field winding is not present. The d-q model parameters are the R-L lumped circuit elements (Figure 6) as viewed from the stator. A detailed development of the d-q model is presented in [7].

3.2. Model application

A second-order d-q model was chosen for the synchronous generator at hand [13]. Its parameters are experimentally identified with two methods: the well-known standstill frequency response (SSFR) tests and the reverse identification method. We then present some simulation results compared to the experimental results.

3.2.1. Parameter values identification from SSFR tests

Test procedures and recommendations when performing SSFR tests are well documented in the IEEE Std 115-2009 [14]. Tests in d- and q-axes are carried out separately in specific rotor positions. The simple network Theory establishes relationships between the d-q model parameters {R_a, L_a, L_{ad}, L_{1d}, R_{1d}, L_{fd}, R_{fd}, L_{aq}, L_{1q}, R_{1q}, L_{2q}, R_{2q}} and six transfer functions known as $Z_d(s)$, $L_d(s)$, $sG(s)$, $Z_{afo}(s)$, $Z_q(s)$, and $L_q(s)$. These transfer functions are evaluated experimentally or by finite element simulation when the exact geometry and material properties of the machine under study are available. Figure 7 shows a comparison between transfer functions obtained from experimental SSFR and from 2D-FE-simulated SSFR using *Flux 2D* by *Cedrat* [15] for the laboratory machine under study. We see that the curves are very similar. It took approximately 18 minute to perform the simulation, while experimental tests needed 3 hour to complete.

For $Z_d(s)$, $L_d(s)$, and $sG(s)$, the field winding is shorted and the rotor is aligned along the direct axis. For $Z_{afo}(s)$, the rotor is in d-axis, but the field winding is left open. Finally, for $Z_q(s)$ and $L_q(s)$, the rotor is short-circuited and aligned along the quadrature axis. Once all the transfer functions are obtained, the model parameters are determined by curve-fitting technique.
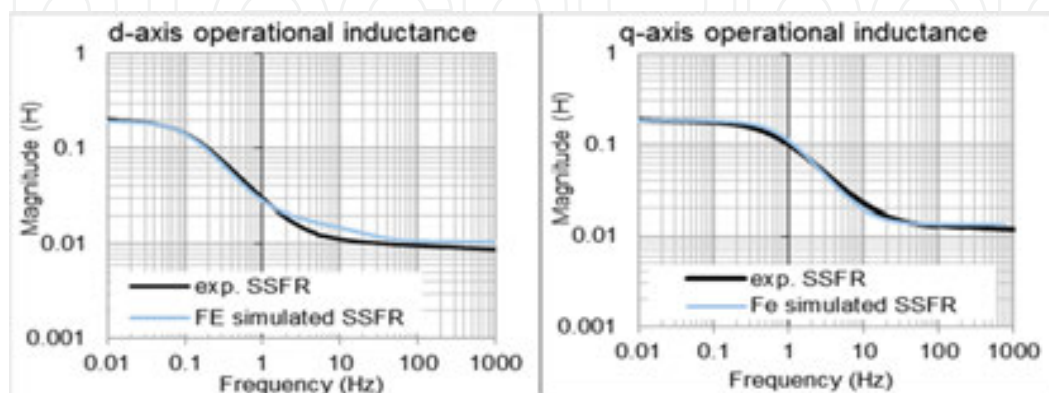

Figure 7: Comparison of experimental and simulated transfer functions

Figure 7. Comparison of experimental and simulated transfer functions

3.2.2. Parameter values identification from reverse identification

The method is based on the analysis of the model's response after a sudden three-phase short circuit and a sudden line-to-line short circuit. These two tests are usually used to fully describe the machine behavior in both axes. From an initial guess of the equivalent circuit parameters {R_a, L_a, L_{ad}, L_{1d}, R_{1d}, L_{fd}, R_{fd}, L_{aq}, L_{1q}, R_{1q}, L_{2q}, R_{2q}}, the tests are simulated using the Matlab/SPS block "SI Fundamental Synchronous Machine." Then the armature and field current waveforms are compared to experimental data in order to calculate the sum of errors

3.2.2. Parameter values identification from reverse identification

The method is based on the analysis of the model's response after a sudden three-phase short circuit and a sudden line-to-line short circuit. These two tests are usually used to fully describe the machine behavior in both axes. From an initial guess of the equivalent circuit parameters $\{R_a, L_a, L_{ad}, L_{1d}, R_{1d}, L_{fd}, R_{fd}, L_{aq}, L_{1q}, R_{1q}, L_{2q}, R_{2q}\}$, the tests are simulated using the Matlab/SPS block "SI Fundamental Synchronous Machine." Then the armature and field current waveforms are compared to experimental data in order to calculate the sum of errors between simulation and experience. The circuit parameters are then iteratively modified using optimization process until the error is minimized.

The machine is modeled by a "SI Fundamental Synchronous Machine" block. It is a d-q model having one equivalent damper winding along d-axis and two equivalent damper windings along q-axis. The nominal field current (I_{fn}) has to be defined as the field current corresponding to nominal voltage on the air gap line (I_{fq}) in order to be consistent with (L_{ad}) and the linear approximation used in this study.

The speed and field voltage supply of the experimental tests must be imposed in the simulation. A clock and lookup tables are used to assign test data values to each simulation time step. The initial rotor position and fault time are chosen such that the experimental and simulated short circuits are synchronized. When the synchronous machine block is used in discrete simulation, a small parasitic resistive load is required at the machine terminals to avoid numerical oscillations. Figure 8 shows the Simulink block diagram used to simulate a short circuit.

The optimization process is implemented with the "fmincon" function of the optimization tool of Matlab. It allows finding the minimum value of constrained nonlinear multivariable problems. There are no particular constraints imposed in the optimization problem, except that all variables must be nonnegative. The field and armature currents of both three-phase and line-to-line short circuits are optimized simultaneously. Results are presented in Table 3.
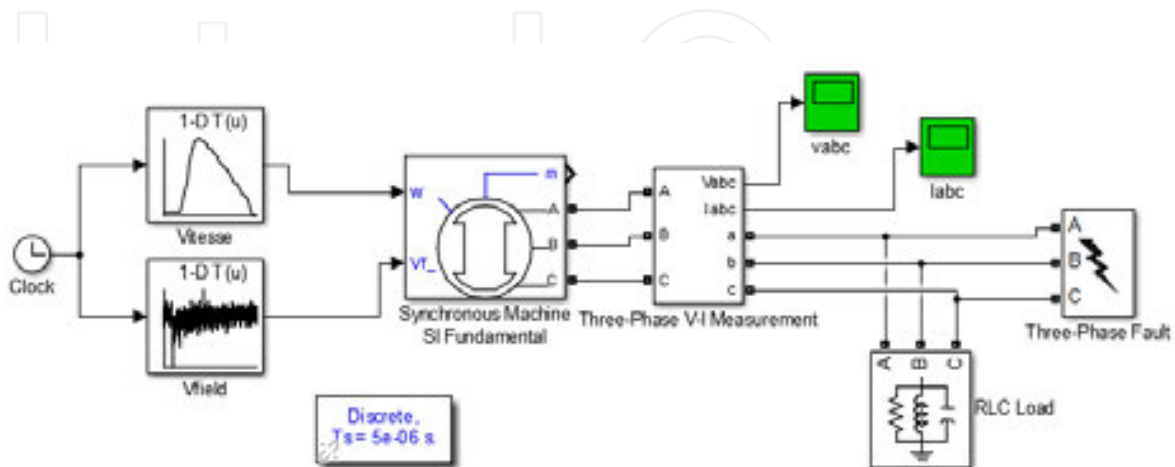

Figure 8. Simulation block diagram

3.3. Validations

The parameters identified by the SSFR and reverse identification methods are presented in Table 3. To evaluate the transient responses of the d-q model, we used the Matlab/Simulink block "SI Fundamental Synchronous Machine" with the parameter values identified using experimental SSFR and reverse identification methods. We compared the field and armature responses to a three-phase short circuit and to a line-to-line short circuit (both with neutral not connected). The field current was approximately equal to 0.22 A (0.44pu). As seen in Figures 9a and 10a, the model is able to reproduce the armature current's waveform. In Figure 10b, the field current's general behavior is well represented. However, the oscillations are less damped in the case of simulated data compared to test data.

Parameter	Experimental SSFR	Reverse identification	SI unit
L_{ad}	171.0	170.6	mH
L_{aq}	176.9	179.0	mH
R_a	156	156	mΩ
L_a	9.1	9.5	mH
R_{fd}	187	186	mΩ
L_{fd}	2.95	2.26	mH
R_{1d}	712	390	mΩ
L_{1d}	0.692	0.113	mH
R_{1q}	1.616	0.871	Ω
L_{1q}	132	0.98	mH
R_{2q}	1.17	2.379	Ω
L_{2q}	3.7	81	mH

Table 3. d-q model parameters of the laboratory machine
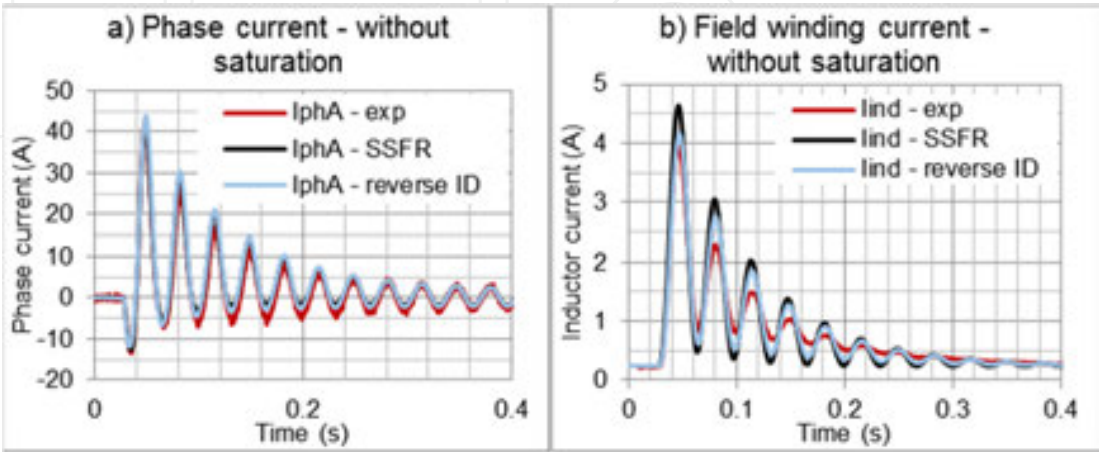
Figure 9. Three-phase short circuit with a field current equal to 0.22 A
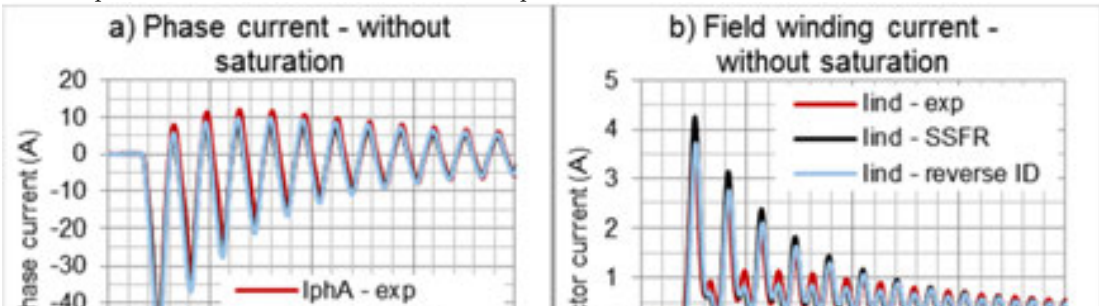
Figure 9: Three-phase short circuit with a field current equal to 0.22 A
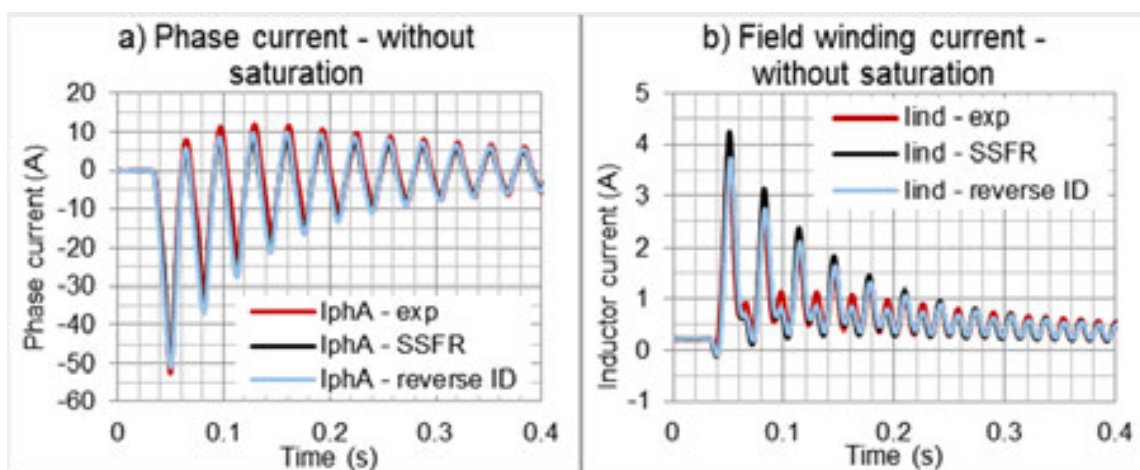
Figure10: Line-to-line short circuit with a field current equal to 0.22 A

Figure 10. Line-to-line short circuit with a field current equal to 0.22 A

4   Coupled-circuit model

generator under study. This method allows the modeling of the magnetic couplings between every electrical circuit in a machine. Compared to the d-q standard model presented earlier, it is a higher-order model that can take account of the spatial harmonics [8].

4.1. Modeling method

The behavior of a polyphase machine can be represented by several electrical circuits that are magnetically coupled. Depending on the discretization level, each individual circuit can be equivalent to a winding or a coil or a conductor or a part of a massive conductor having a constant current density. Generally, the selected circuits correspond to the stator phases, the rotor field, and the rotor damper winding [16]. The magnetic saturation is not taken into account in this section, but an improvement of the model using a simple method is presented in section 6.

The method we present does not introduce a reference frame transformation and the stator has a fixed angle. Each electrical circuit is linear and can be modeled by a resistance and several inductances that depend on the rotor angular position θ. The mutual inductances between the stator and the rotor alternate relative to the rotor position. Other inductances may also vary around a mean value relative to the space harmonics caused by rotor or stator slotting or saliency.

The set of circuit equations can be written in a vector matrix form as shown in (1). The elements of matrix $L(\theta)$ provide the magnetic couplings in the stator, in the rotor, and between them (2):

$$[V] = [R][I] + \frac{d\{[L(\theta)][I]\}}{dt} \tag{1}$$

$$L(\theta) = \begin{bmatrix} [L_S]_{n \times m} & [M_{RS}]_{n \times m} \\ [M_{RS}]_{m \times n} & [L_r]_{m \times n} \end{bmatrix} = \begin{bmatrix} \begin{bmatrix} L_{s1} & M_{s12} & \cdots & M_{s1n} \\ M_{s21} & \ddots & \ddots & \vdots \\ \vdots & \ddots & \ddots & M_{sn-1n} \\ M_{sn1} & \cdots & M_{snn-1} & L_{sn} \end{bmatrix} & \begin{bmatrix} M_{s1r1} & M_{s1r2} & \cdots & M_{s1rm} \\ M_{s2r1} & \ddots & \ddots & \vdots \\ \vdots & \ddots & \ddots & M_{sn-1rm} \\ M_{snr1} & \cdots & M_{snrm-1} & M_{snrm} \end{bmatrix} \\ \begin{bmatrix} M_{r1s1} & M_{r1s2} & \cdots & M_{r1sn} \\ M_{r2s1} & \ddots & \ddots & \vdots \\ \vdots & \ddots & \ddots & M_{rm-1sn} \\ M_{rms1} & \cdots & M_{rmsn-1} & M_{rmsn} \end{bmatrix} & \begin{bmatrix} L_{r1} & M_{r12} & \cdots & M_{r1m} \\ M_{r21} & \ddots & \ddots & \vdots \\ \vdots & \ddots & \ddots & M_{rm-1m} \\ M_{rm1} & \cdots & M_{rmm-1} & L_{rm} \end{bmatrix} \end{bmatrix} \tag{2}$$

To represent the movement and the variation of current, we may express (1) in the following manner, where Ω is the rotor angular speed:

$$[V] = [R][I] + \Omega \left\{ \frac{d[L(\theta)]}{d\theta_m} \right\} [I] + [L(\theta)] \left\{ \frac{d[I]}{dt} \right\}. \tag{3}$$

The voltage on each circuit must be imposed to solve (3) and find the derivative of all currents (4):

$$\frac{d[I]}{dt} = [L(\theta)]^{-1} \cdot \left[[V] - \left([R] + \Omega \frac{d[L(\theta)]}{d\theta_m} \right)[I] \right] \tag{4}$$

The circuit equations to account the stator star or delta connection and the damper bars connected in a grid or cage design. Figure 11 presents an example of circuit for the rotor damper bar connections connected by shorting-ring impedances (R_{ri}, L_{ri}) in a cage design. The unknowns of the circuit problem are the mesh currents (J_i), and the matrix $[L(\theta)]$ and $[R]$ must be modified as detailed in Ref. [16].

Now that the circuit model is defined, the values of the inductance $[L(\theta)]$ and resistance $[R]$ matrix have to be identified. The identification of the resistance matrix is straightforward and depends on the section of the conductor and its length. The values in the inductance matrix must be identified for a given number of angular positions (θ). Some authors propose an analytical approach to estimate the inductance curves using winding functions [8, 17]. It assumes that the permeance of iron is infinite. Another way to avoid additional simplifications is to use a finite element method [18], as proposed in this study.

For analysis purposes, the time required for this identification is quite well compensated by its increased precision. The identification is done with 2D finite element simulation with static
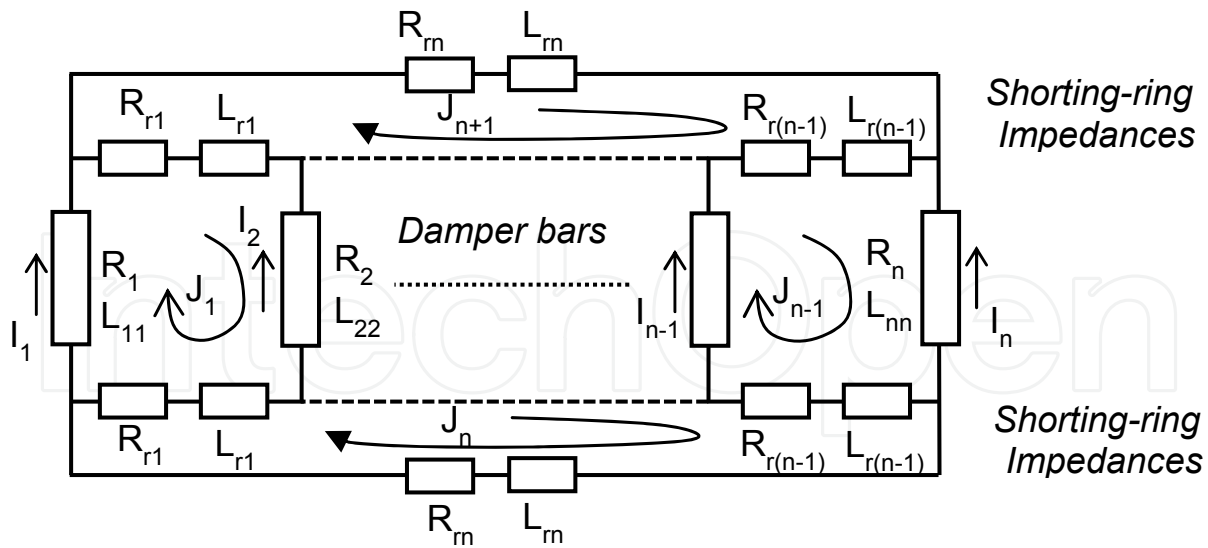
Figure 11. Equivalent circuit for a rotor cage for the damper winding

Now that the circuit model is defined, the values of the inductance [$L(\theta)$] and resistance [R] matrix have to be identified. The identification of the resistance matrix is straightforward and depends on the section of the conductor and its length. The values in the inductance matrix must be identified for a given number of angular positions (θ). Some authors propose an analytical approach to estimate the inductance curves using winding functions [8], [17]. It assumes that the permeance of iron is infinite. Another way to avoid additional simplifications is to use a finite element method [18], as proposed in this study.

For analysis purposes, the time required for this identification is quite well compensated by its increased precision. The identification is done with 2D finite element simulation with static magnetic field resolution. The permeability of the magnetic material must be a constant (no magnetic saturation) and the extremity effects (magnetic flux leakage in the third direction) are neglected. They could be considered in a 3D simulation. This method allows a fast, general, and accurate identification of the inductance curves.

From the inductance curves, we can evaluate their first and second derivatives curves [18]. Linear interpolation in these curves is an efficient method to estimate the inductance value and its derivative value for any rotor position. Knowing the inductance values of two discrete rotor positions (θ_0 and θ_1), one can compute the inductance value for any rotor position θ between θ_0 and θ_1 using (5):

$$\text{for } \theta_0 < \theta \le \theta_1 \quad L(\theta) = L(\theta_0) + (\theta - \theta_0) \cdot \frac{L(\theta_1) - L(\theta_0)}{\theta_1 - \theta_0} \tag{5}$$

The coupled-circuit model can easily be implemented in Matlab-Simulink that provides many numerical methods to solve the set of differential equations. A variable-step solver like a fifth-order ode15s is efficient in terms of simulation time, accuracy, and stability. The simulation time is also improved using the rapid accelerator mode of Simulink. The linear interpolation in a table of discrete values is easy to implement with the Simulink tools. Using an identification of inductance curves with 2D FEM, the coupled-circuit model has the advantage of combining the precision of the finite element spatial representation for the magnetic couplings, with high efficient variable-step solvers.

similar to the one used in finite element simulation to simulate the currents in massive conductors as the current density in a cell area is constant.

It seems not practicable to estimate the magnetic losses with this kind of model. However, the user can add some search coils in the different parts of the machine, which can be used as flux sensors. With that information, one can evaluate the magnetic losses with the Bertotti formula. The addition of search coils does not make the study more difficult as all the magnetic couplings are calculated with the finite element method. This increases slightly the order of the model.

4.2. Coupled-circuit model application

To evaluate the inductance curves of the generator under study, we used a 2D finite elements software (Flux 2D of Cedrat [15]). To reduce the size of the study domain, and reduce the simulation time required for inductance identification, the magnetic periodicity is considered. In this case, users should control the multiplying factors and calculate the inductances for a machine part only. This management of multiplying factors is simple to integrate in the coupled-circuit model. This allows more options for the winding connections between different parts of the machine.

The generator under study has a magnetic periodicity on half of its domain. Consequently, we have to identify 16 coupled circuits: 3 circuits for the stator phases, 1 circuit for the field, and 12 circuits for the damper bars. Thus, the skin effect in the damper bars is neglected. The number of rotor positions should be chosen high enough to allow the representation of the no-load voltage harmonic content. The influence of the discretization of the inductance curves with different numbers of rotor positions (20, 10, and 5 rotor positions per stator slot pitch) is analyzed in [18]. The use of 20 rotor positions within one stator slot pitch allows a very precise prediction of the harmonics due to the slot pulsation field. However, the shapes are quite well preserved even with five rotor positions per stator slot pitch. The higher harmonic content can be readily seen on the curve of the field self-inductance.

4.3. Validations

This section compares the waveforms obtained with the coupled-circuit model to the experimental ones.

The no-load voltage of the generator has an important harmonic content (third harmonic in the line-neutral voltage waveform and slot harmonic). The model is able to reproduce the shape of the curves accurately, but there is a small difference on the signal amplitude caused by the linear permeability used in the FE model (Figures 12 and 13).

When all phase ends are short-circuited with themselves, the phase current is trapezoidal (Figure 14) because of the third harmonic of the no-load voltage. Figure 15 presents the current waveform of a sustained three-phase short circuit, with a star connection and without the neutral–ground connection. In that case, the harmonic current multiples of three cannot circulate and the shape of the short-circuit current becomes more sinusoidal. The simulated waveforms are similar to the experimental data for both cases.
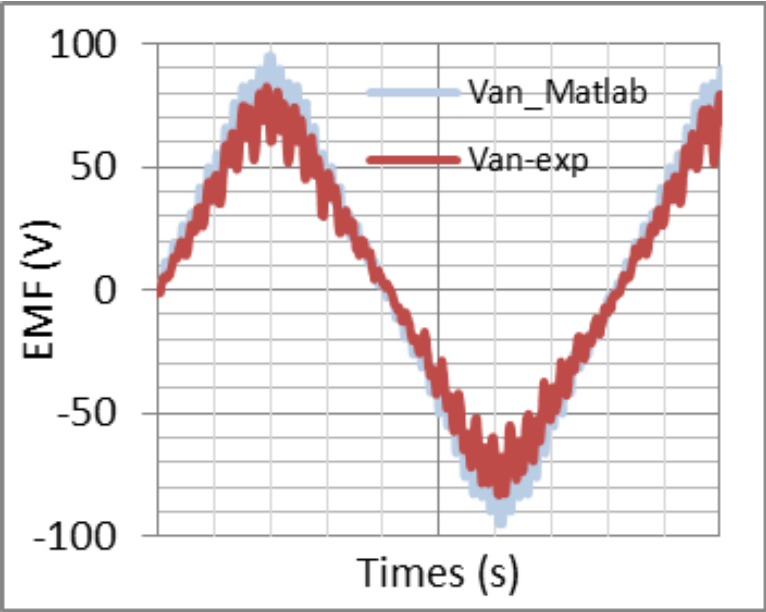
Figure 12. No-load voltage (V_{LN}) (field-winding current: 0.22 A; speed: 914 rpm)
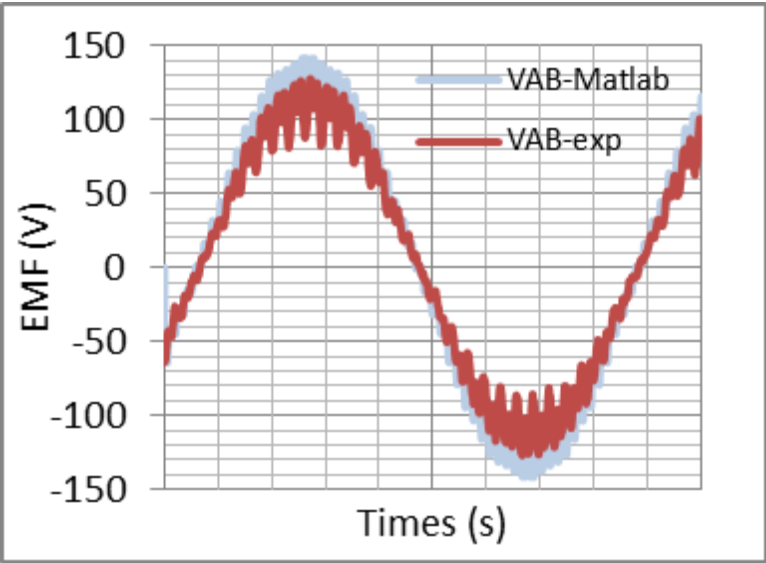

Figure 13. No-load voltage (U_{LL}) (field-winding current: 0.22 A; speed: 914 rpm)

Here, we compare the sudden short-circuit response of every phase with itself. To compare the transient responses, we have synchronized the signals and imposed the experimental speed and field voltage. Prior to the sudden short circuit, the machine is operated at 914 rpm without load and the field current is 0.22 A (0.44 pu). At this point of operation, the magnetic saturation is negligible. Figure 16 compares the response of the phase and field current during the transient. The waveforms are well reproduced by the simulation. The current overshoot is around 2 pu for the stator winding and 8 pu for the field winding.
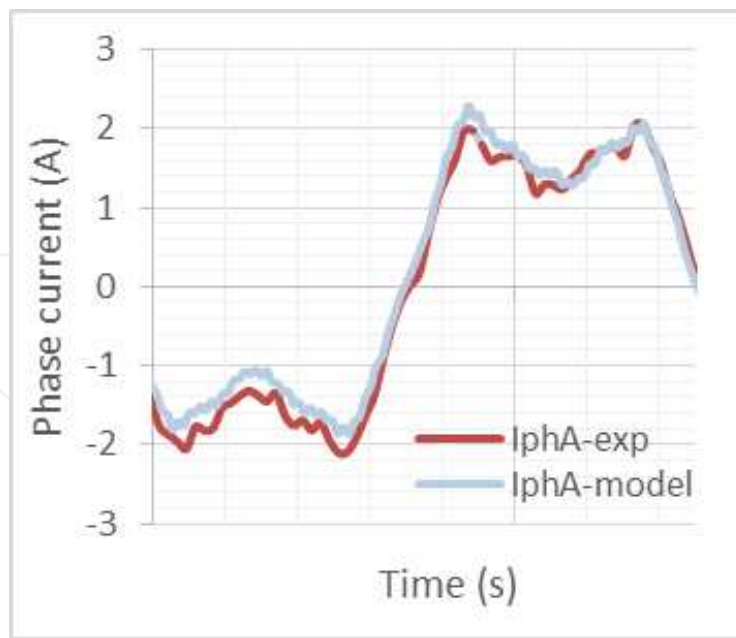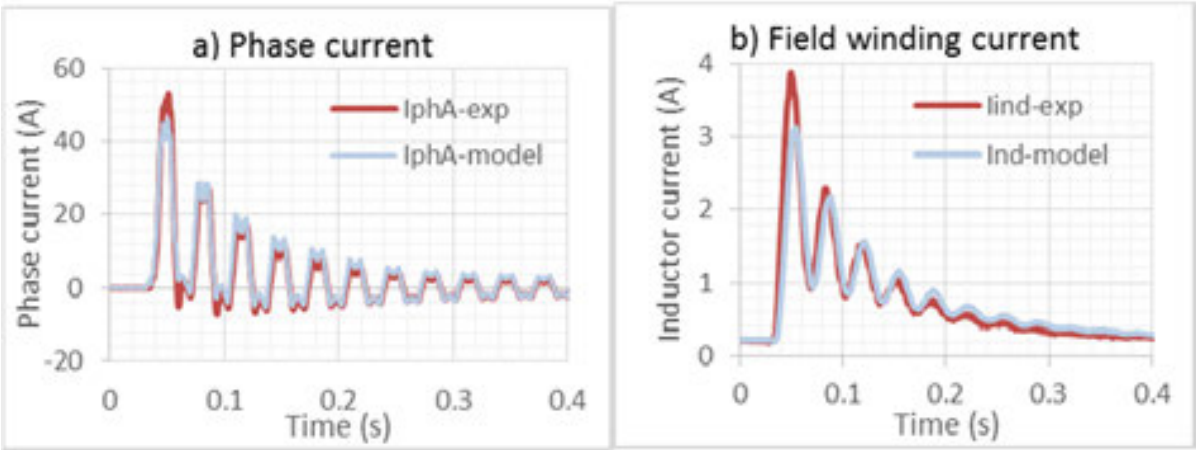
Figure 14. Steady-state current with each stator phase shorted to itself
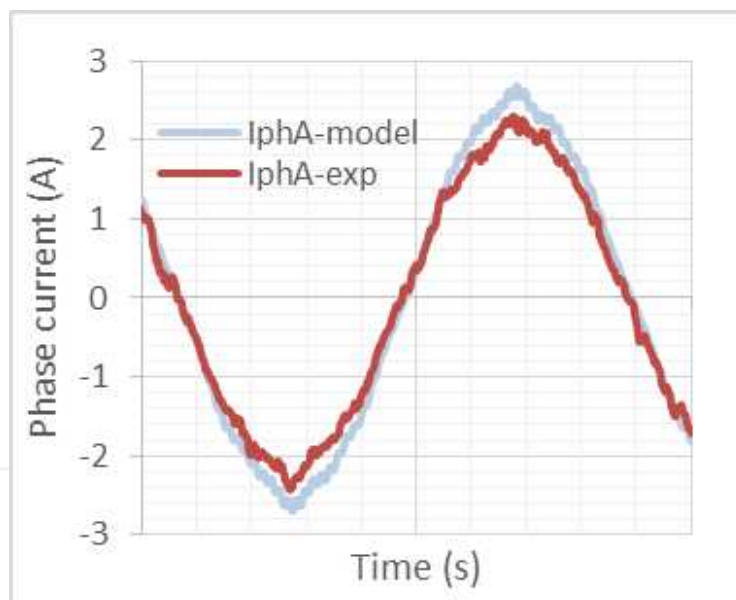
Figure 15. Steady-state current with shorted star connection

Figure 17 compares the results of a three-phase short circuit without the neutral connection. The currents and the time constant are nearly the same as in Figure 16, but the shape of the phase current is more sinusoidal.

A phase-to-phase short circuit is presented in Figure 18. This short circuit generates a negative sequence current in the stator that induces an alternative voltage at twice the stator electrical frequency in the rotor winding. This explains the field current oscillations at the end of the transient period.

the transient responses, we have synchronized the signals and imposed the experimental speed and field voltage. Prior to the sudden short circuit, the machine is operated at 914 rpm without load and the field current is 0.22 A (0.44 pu). At this point of operation, the magnetic saturation is negligible. Figure 16 compares the response of the phase and field current during the transient. The waveforms are well reproduced by the simulation. The current overshoot is around 2 pu for the stator winding and 8 pu for the field winding.

Figure 16: Transient currents when each stator phase is short-circuited to itself

Figure 17 compares the results of a three-phase short circuit without the neutral connection.
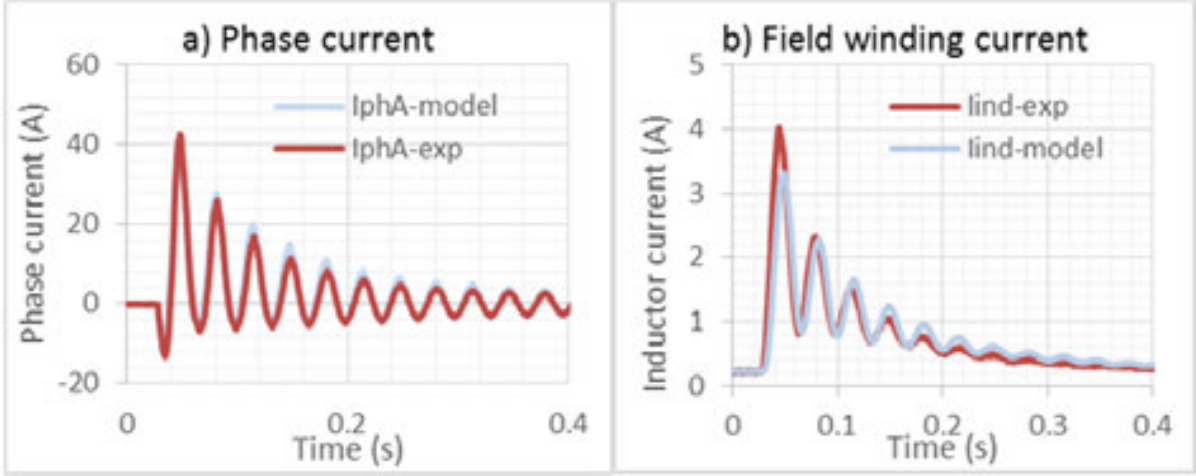
Figure 17: Transient currents for a three-phase short circuit without neutral connection

A phase-to-phase short circuit is presented in Figure 18. This short circuit generates a negative sequence current in the stator that induces an alternative voltage at twice the stator electrical frequency in the rotor winding. This explains the field current oscillations at the end of the transient period.
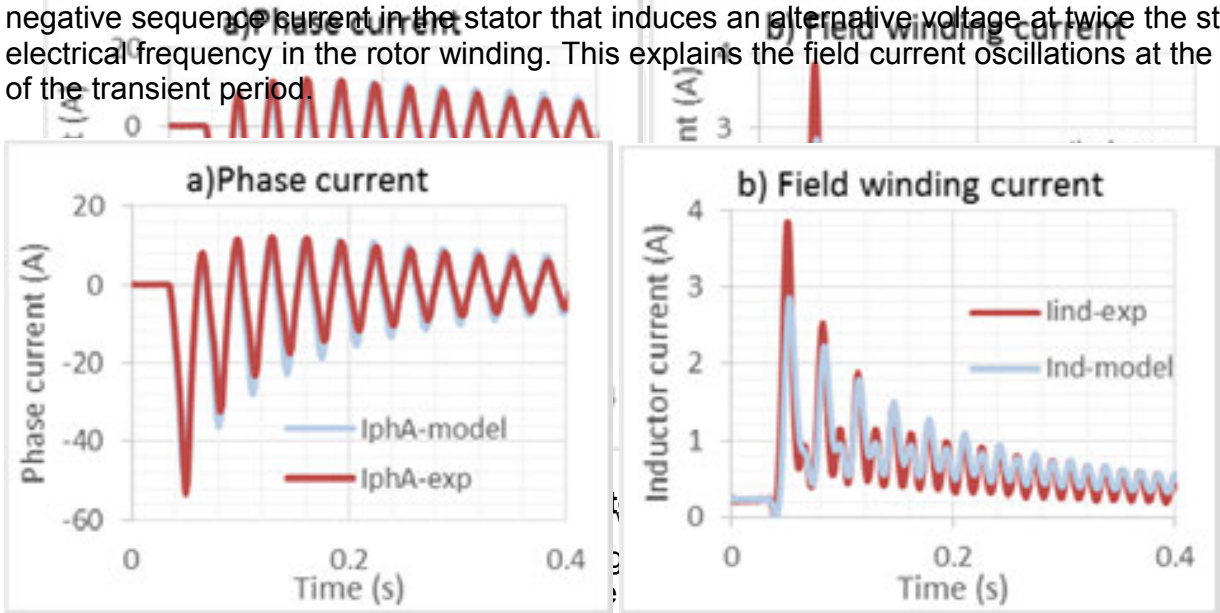
Figure 18: Transient currents for line-to-line short circuit without neutral connection

These results show that the coupled-circuit model is very performant to simulate various transient responses by taking into account the time and space harmonics of the machine. The assumptions that neglect the magnetic saturation and the skin effect in the damper circuit appear to be valid with a low field current (044 pu). Comparisons with a higher field current (1 pu) are presented in section 7 for all the proposed models.

If we add a neutral connection to the ground, current harmonic multiples of three can circulate and the shape of the phase current is trapezoidal (Figure 19). This is also true for a single-phase short circuit (Figure 20).

If we add a neutral connection to the ground, current harmonic multiples of three can circulate and the shape of the phase current is trapezoidal (Figure 19). This is also true for a single-phase short circuit (Figure 20).

These results show that the coupled-circuit model is very performant to simulate various transient responses by taking into account the time and space harmonics of the machine. The assumptions that neglect the magnetic saturation and the skin effect in the damper circuit appear to be valid with a low field current (0.44 pu). Comparisons with a higher field current (1 pu) are presented in section 7 for all the proposed models.
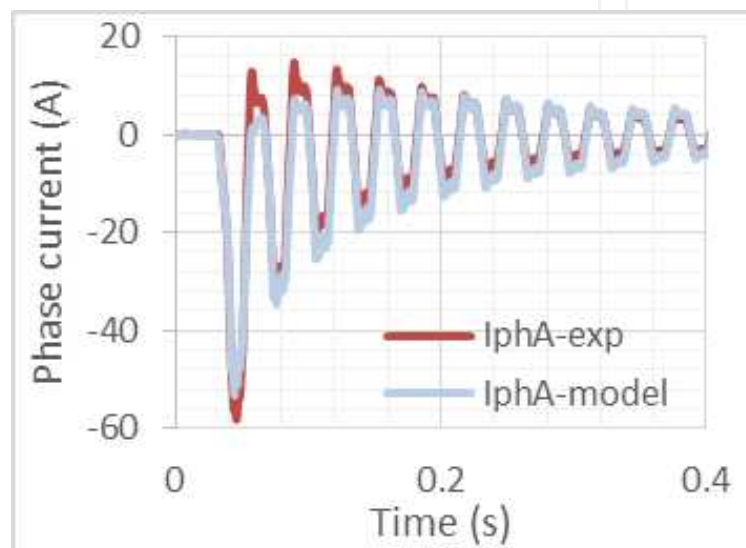
Figure 19. Line-to-line short circuit with neutral connection
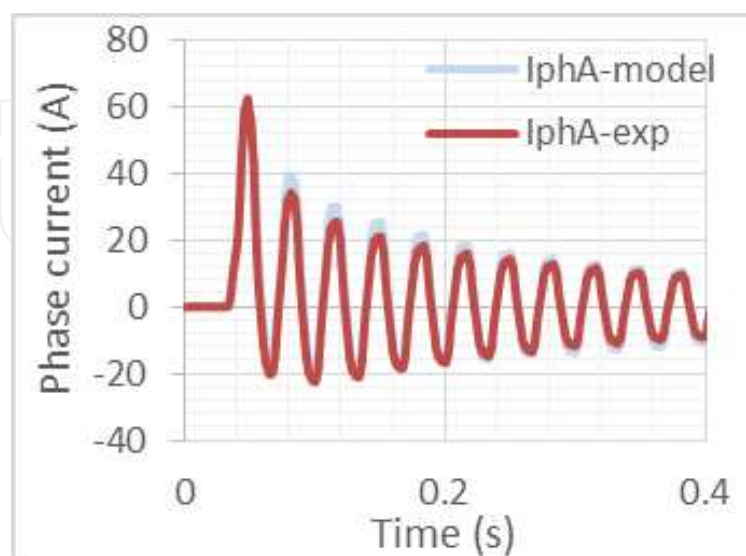
Figure 20. Phase current with one phase shorted to the neutral

5. Finite element model

The electromagnetic field computation based on Maxwell's equations using the finite element method is the state of the art in high-precision modeling of electrical machine. While being precise, it is the highest time-consuming simulation method. For the simulation of electrical machines, it is generally assumed that the displacement currents can be neglected and the electromagnetic problem can be studied with magnetostatic or magnetodynamic simulations [12]. This section discusses the modeling method and compares the simulation results of generator under study to the experimental measurements.

5.1. Modeling method

Most electrical machines can be studied with a 2D approximation [12]. That approximation is valid when the geometry of a machine section does not change along the axial direction. The problem is solved using the magnetic vector potential that has only one component in the z direction. Some boundary conditions (Dirichlet, Neumann, periodicity, etc.) also minimize the size of the study domain. Finite element simulation can consider the movement of the rotor, $B(H)$ curves of nonlinear magnetic materials, and massive conductor (proximity and skin effects). The conductors can be connected to each other's with an external electrical circuit. The currents in all conductors and the copper losses can be calculated with greater precision. For a given rotor position, it is also possible to calculate the torque by the Maxwell stress tensor or the virtual works and to estimate the magnetic losses in the machine. Time-stepping computations are based on Euler method using a fixed time step. More details on the finite element method applied to electrical machines are provided in [12].

5.2. Model application

We used a commercial software, Flux 2D of Cedrat [15], for the finite element modeling of the generator. Figure 21 shows the periodic 2D sketch of the resolution domain. Massive conductors of the damper winding are modeled using the copper conductivity. The external circuit links the damper bars with constant resistances that represent the contact resistances and the shorting ring.

5.3. Validations

To consider the magnetic saturation, we used an analytic saturation curve [15]. This is a combination of a straight line and an arc tangent curve made with two parameters ($\mu_r = 4000$, $B_s = 1.5$ T). The stator and rotor are made of the same magnetic material. The simulations are made in magnetodynamic with a fixed time step of 0.25 ms (135 pts per electrical period at 30 Hz). The experimental speed variations and the field voltage are imposed as inputs. Experimental stator voltage waveforms are also imposed after the sudden short circuit.

The steady-state waveforms of no-load electromotive force (emf) and short-circuit phase current with or without neutral connection are very close to the experimental results, and that is true for all points of operation; the saturation is well represented. We compare the same
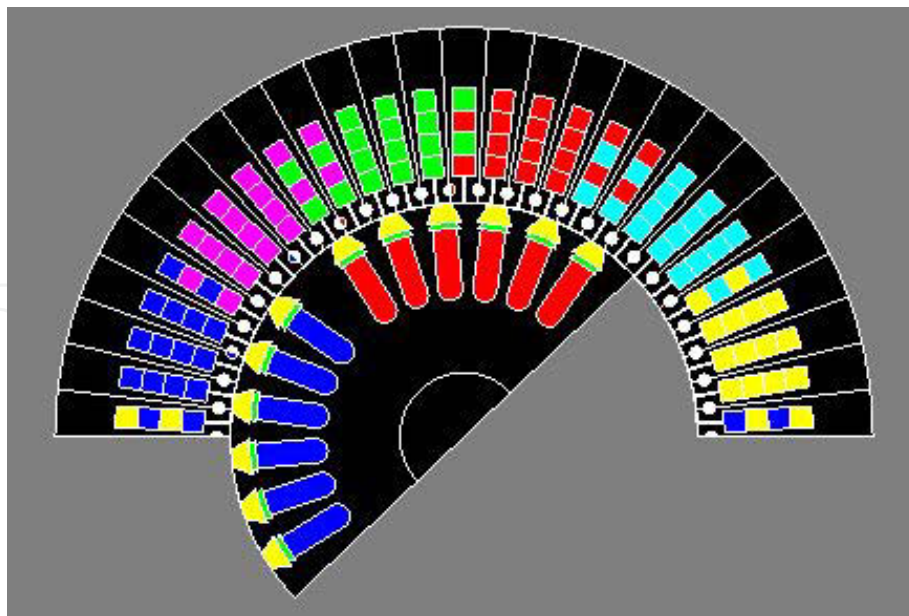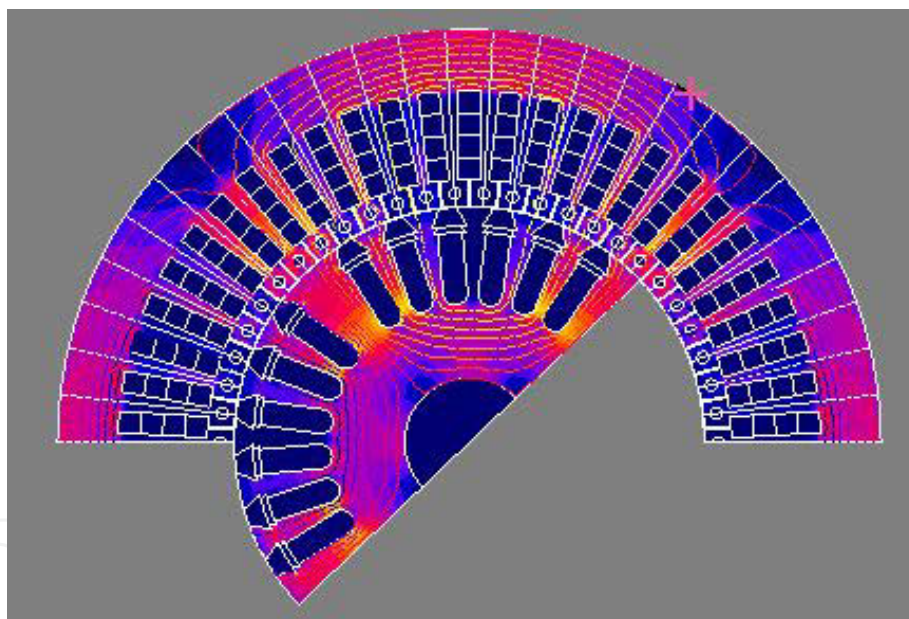
Figure 21. 2D transverse sketch

Figure 22. Flux densities (if = 0.22 A)

results as for the previous models using the experimental waveforms with a field current of 0.22 A (0.44 pu). The phase current transient responses during a three-phase short circuit (Figure 23) and a two-phase short -circuit (Figure 24) are compared to the experimental measurements. By comparing these results with the ones obtained with the previous models, it can be seen that the shape of the signals (peak value, time constant, oscillations) is always well reproduced. The most significant difference is observed on the oscillation amplitude of the field current during a line-to-line short circuit (Figure 24b).

(Figure 23) and a two-phase short -circuit (Figure 24) are compared to the experimental measurements. By comparing these results with the ones obtained with the previous models, it can be seen that the shape of the signals (peak value, time constant, oscillations) is always well reproduced. The most significant difference is observed on the oscillation amplitude of the field current during a line-to-line short circuit (Figure 24b).
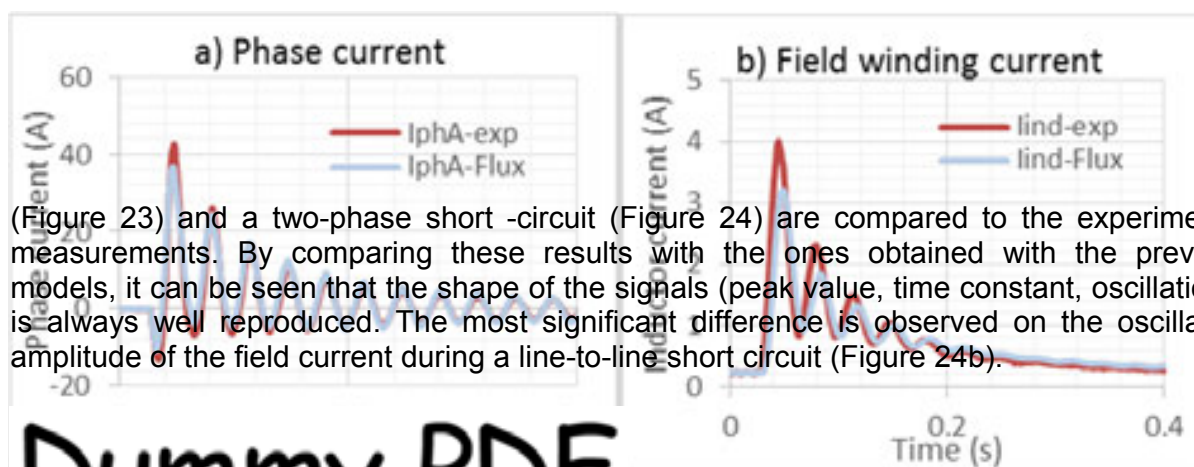
Figure 8: Phase current of a sudden three-phase short circuit without neutral
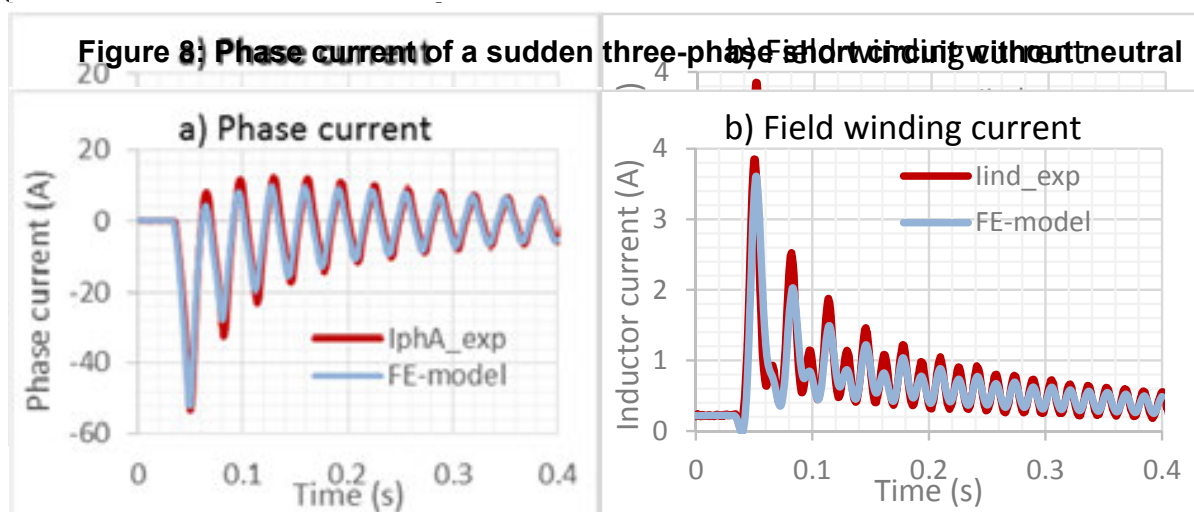
Figure 24: Transient currents for line-to-line short circuit without neutral

6   Improved circuit models considering magnetic saturation

In synchronous machines, magnetic saturation is clearly visible on the no-load characteristic. It is possible to approximate the no-load characteristic with the air gap line and neglect the saturation phenomenon for machine operations with a low field current. We have shown that this approximation is valid for the transient simulation of the generator with a field current equal to 44% of its nominal value.

When the saturation takes effect, that approximation is no longer true [20]. The no-load voltage amplitudes are greatly overestimated with a linear model, and this leads to incorrect steady-state and transient simulation results. Figure 25 compares the field current response of both circuit models (d-q and coupled circuits) during a three-phase short circuit at the nominal field current (0.5 A). The current waveforms obtained are less damped than the experimental result. This overestimation of the currents leads to incorrect prediction of losses and transient torques.
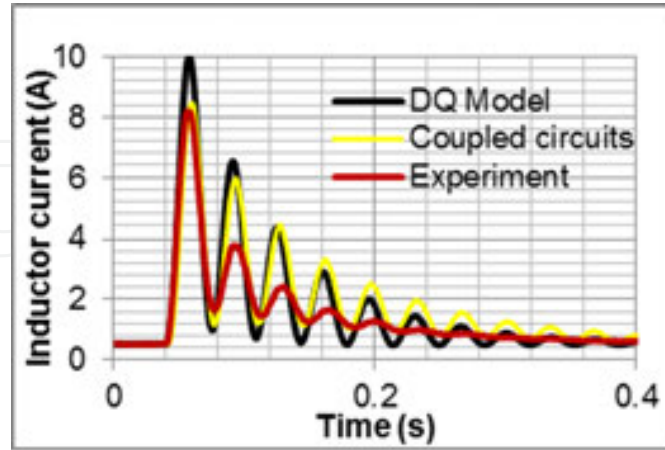
current (0.5 A). The current waveforms obtained are less damped than the experimental result. This overestimation of the currents leads to incorrect prediction of losses and transient torques.

Figure 25. Overestimation of field current without considering the saturation

Many methods are proposed to take into account the magnetic saturation in the d-q model [7, 20-22]. It is generally assumed that the leakage inductance does not vary regarding the level of saturation. Only the magnetizing inductances ($B(H)$, L_{ad}) are affected. It is also assumed that the stator armature reaction has no influence on the magnetic saturation. Consequently, the magnetic saturation can be deduced from the machine no-load operation.

The simplest method uses two saturation factors (L_{aq}, k_{sd}) to modify the value of the magnetizing inductances (k_{sq}, L_{ad}) (6). The factor (L_{aq}) is function of the excitation current (k_{sd}). It is computed from the no-load characteristic and the air gap line. For a given field current, we compute the ratio between the no-load voltage (i_f) and the equivalent voltage on the air gap line: E_v(7).

$$\begin{cases} L_{adsat} = k_{sd}(i_f) \cdot L_{ad} \\ L_{aqsat} = k_{sq}(i_f) \cdot L_{aq} \end{cases} \tag{6}$$

$$k_{sd}(i_f) = \frac{E_v(i_f)}{E_{linear}(i_f)}. \tag{7}$$

For the salient pole machine, the coefficient ($k_{sd}(i_f) = \frac{E_v(i_f)}{E_{linear}(i_f)}$.) is usually set equal to 1 for all operating conditions as the path of q-axis flux is mostly in the air [7]. In the case of round rotor alternator, the coefficient (k_{sq}) is often assumed equal to (k_{sq}) as the q-axis saturation data are usually not available. In reality, magnetic saturation creates a cross-coupling between d- and q-axes [22]. However, the differences in stability performance when considering cross-magnetization have not been demonstrated for large generators [7]. In the case of the coupled-

circuit model, we have applied the same simplified method using only one saturation coefficient equal to (k_{sd}). All parameters of the inductance matrix have been multiplied by this coefficient.

For the generator under study, we computed the variations of (k_{sd}) using the no-load characteristic up to twice the nominal field current. When the field current is greater than this value, the saturation coefficient is kept constant at its smallest value.

Figure 26 presents the simulation results when the magnetic saturation is taken into account. The d-q model current response is improved, but it is the coupled-circuit model that provides the best results. This improvement is impressive as the magnetic saturation is roughly taken into account.
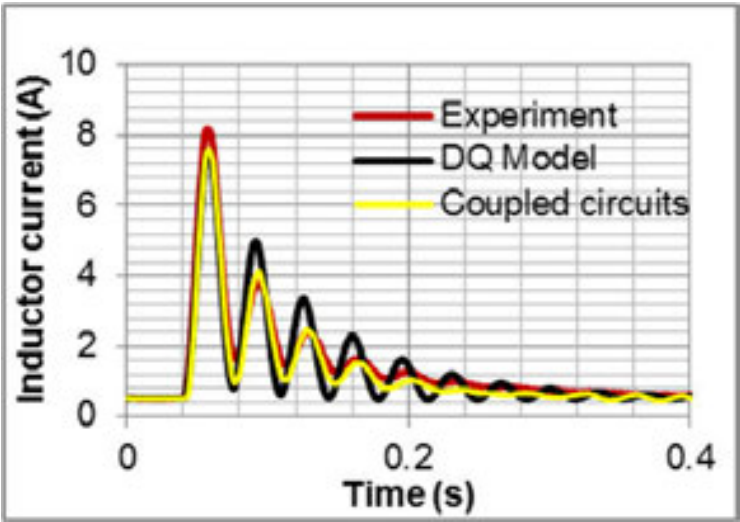
Figure 26. Field current when considering the saturation

Note that the field current peak reaches 16 times its nominal value. At that specific moment, the finite element analysis shows that the magnetic saturation is predominantly located in the stator and rotor tooth tips because of the magnetic stator reaction (Figure 27).
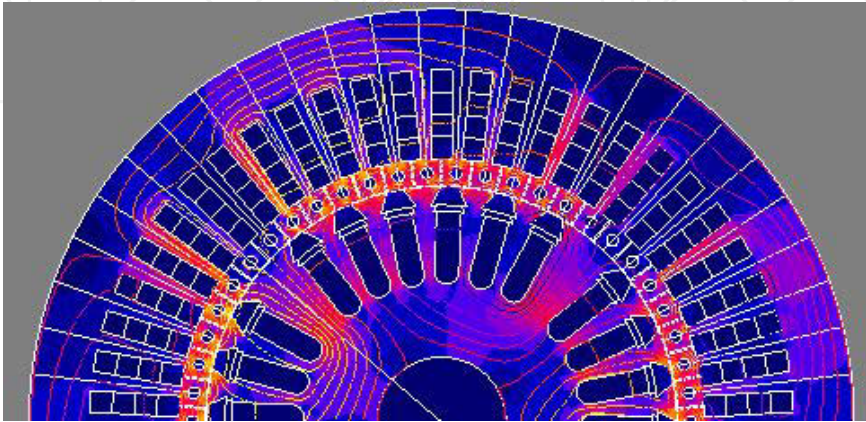
Figure 27. Magnetic flux densities at 0.055 s (field current peak)

7. Sudden short-circuit comparisons

This section compares the ability of the d-q, coupled-circuit, and finite element models to reproduce the current responses during sudden short circuits. We consider four kinds of short circuits: the sudden two-phase and three-phase short circuits without neutral connection, a two-phase short circuit with neutral–ground connection, and a single-phase short circuit with neutral–ground connection. We also compare several waveforms that have not been measured like the damper bar currents, the electromagnetic torque, and the damper circuit losses.

7.1. Three-phase short circuit without neutral connection at full voltage

Right before both sudden short circuits, the machine is at 900 rpm without load and at rated field current. Solely for the purpose of comparing the current waveforms, the experimental rotor field voltage waveform and the experimental speed are used as inputs in the simulations. In addition, at the moment of the short circuit and until the end of the simulation, the measured voltage at the short circuit (at the breaker terminals) is applied in the simulation. The initial values for the rotor position and field current are imposed to the experimental ones. The time required for the simulation is of a few seconds for the d-q model, 15 second for the coupled circuit, and 2 hour 45 minute for the FE simulation. Figures 28 to 30a compare the phase current during the three-phase short circuit.

The experimental phase current peaks at 7 pu during this short circuit. The response of the d-q and the coupled-circuit models are similar, and the differences with the experimental waveforms appear to be related to the speed variations and the precision on the initial conditions. Other factors could cause this difference such as magnetic saturation and skin effect. The finite element simulation is more accurate to consider these phenomena, but there is no significant improvement on the phase current response. The fixed step, the simple Euler method, and the precision of material properties could explain the discrepancies. The moment of the short circuit is between two time steps of 0.25 ms. Figure 30b shows the field current waveform that can be compared to Figure 26.

When comparing the waveforms of damper bar currents (Figure 31), it can be seen that the result of the coupled-circuit model matches closely with those of the finite elements. The d-q model does not provide that information. The experimental damper bar currents were not measured on the generator.

A comparison of simulated electromagnetic torque is shown in Figure 32. Figure 33 is a comparison of total copper losses in the damper bar circuit.

As the d-q model neglects all voltage and slotting harmonics, the high-frequency torque oscillations are filtered (Figure 32). The torque calculation methods of the two other models (FE and coupled circuit) lead to similar waveforms. It suggests that the electromagnetic torque peaks at 180 Nm (6.4 pu) compared to 110 Nm for the d-q model. One can also conclude that the assumptions used in the coupled-circuit model are valid. The finite element method takes account of the skin effect in the bars. This explains that the damper losses are near twice larger than the other models' estimations (Figure 33).
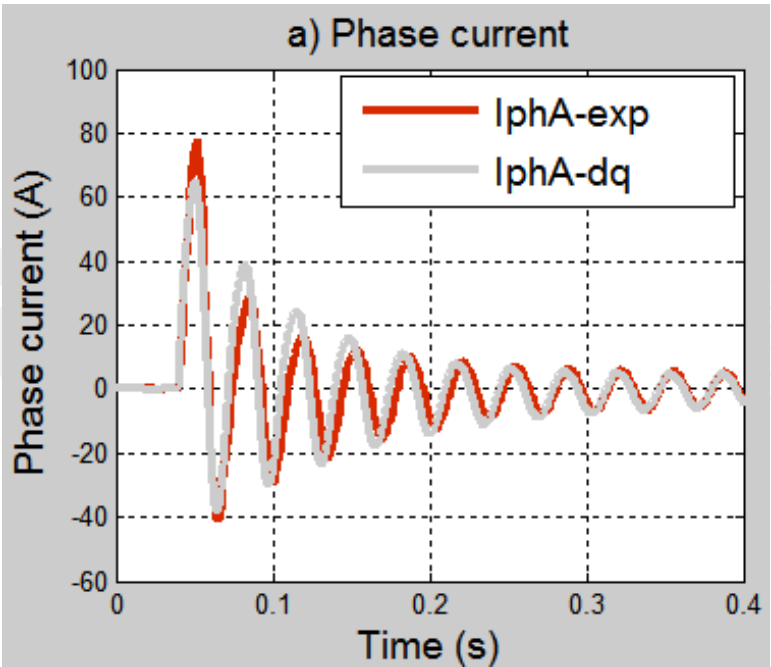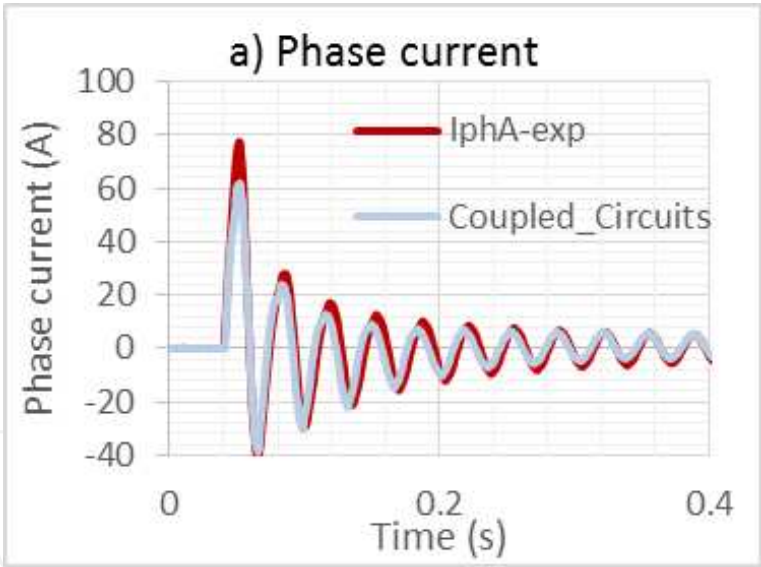
Figure 28. d-q model/experiment

Figure 29. Coupled circuit/experiment

7.2. Two-phase short circuit without neutral connection at full voltage

The same conditions are used for the simulation of the sudden two-phase short circuit as for the previous section on the sudden three-phase short circuit.

From Figures 34 to 36, the phase and field currents are compared. A similar error can be seen on the evaluation of the first current peak. The possible advantage of a finite element simulation in obtaining these current waveforms is not entirely clear.

Figure 11: Two-phase short circuit; coupled circuit model vs experiment
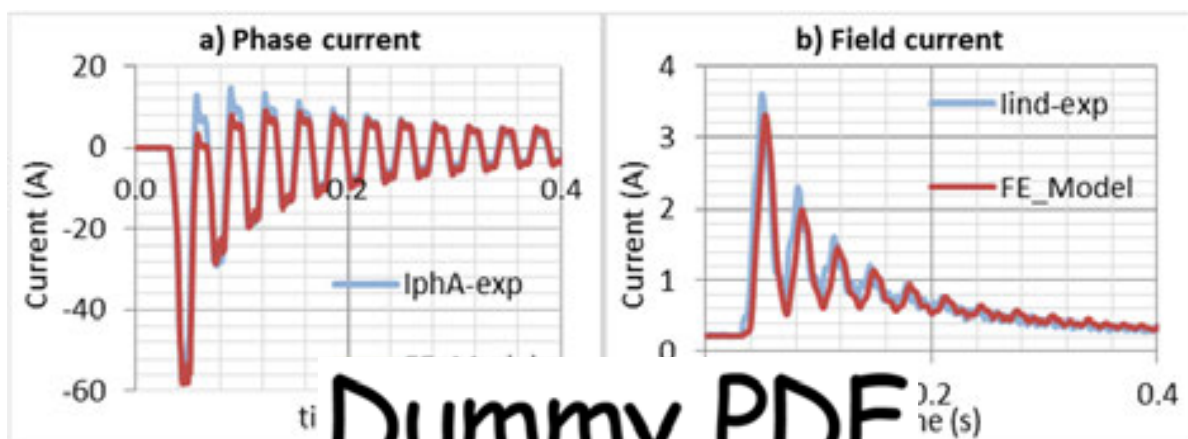
a) Phase current
b) Field current

Figure 12: Two-phase short circuit; finite element model vs experiment

Figure 30. Three-phase short circuit; finite element model vs experiment

Figure 30: Three-phase short circuit; finite element model vs experiment

a) Damper bar 1
b) Damper bar 6

a) Damper 1 current
b) Damper 6 current
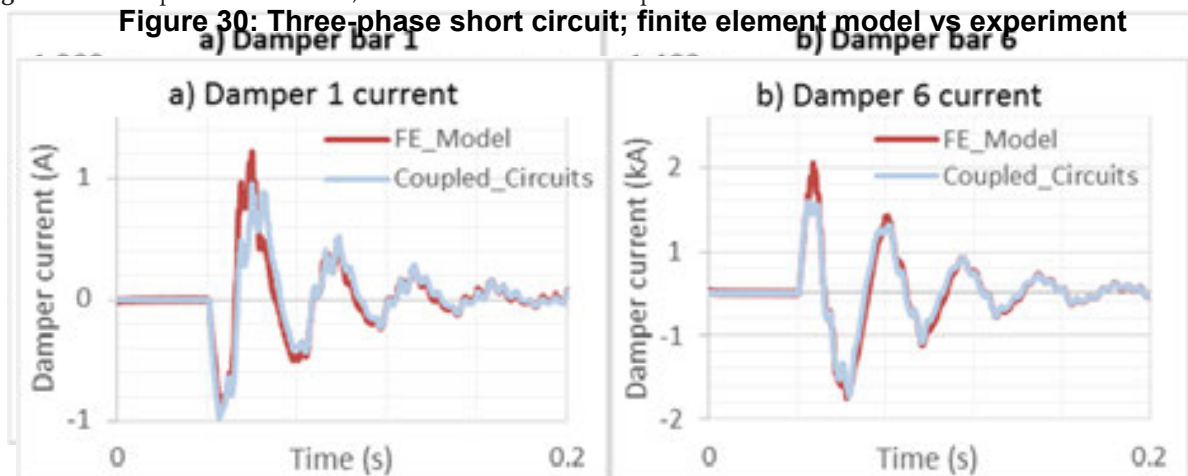
Figure 13: Two-phase short circuit; damper bar currents

Figure 31: Three-phase short circuit; damper bar currents

Figure 31. Three-phase short circuit; damper bar currents

When comparing the waveforms of damper bar currents (Figure), it can be seen that the result of the coupled circuit model are close to finite elements. The d-q model does not currents were not measured on the phase short circuit as for the previous first cycle of the phase current measurements

7.4. Single-phase to ground short circuit

The same condition

A comparison (Figure 44a). He is a comparison of
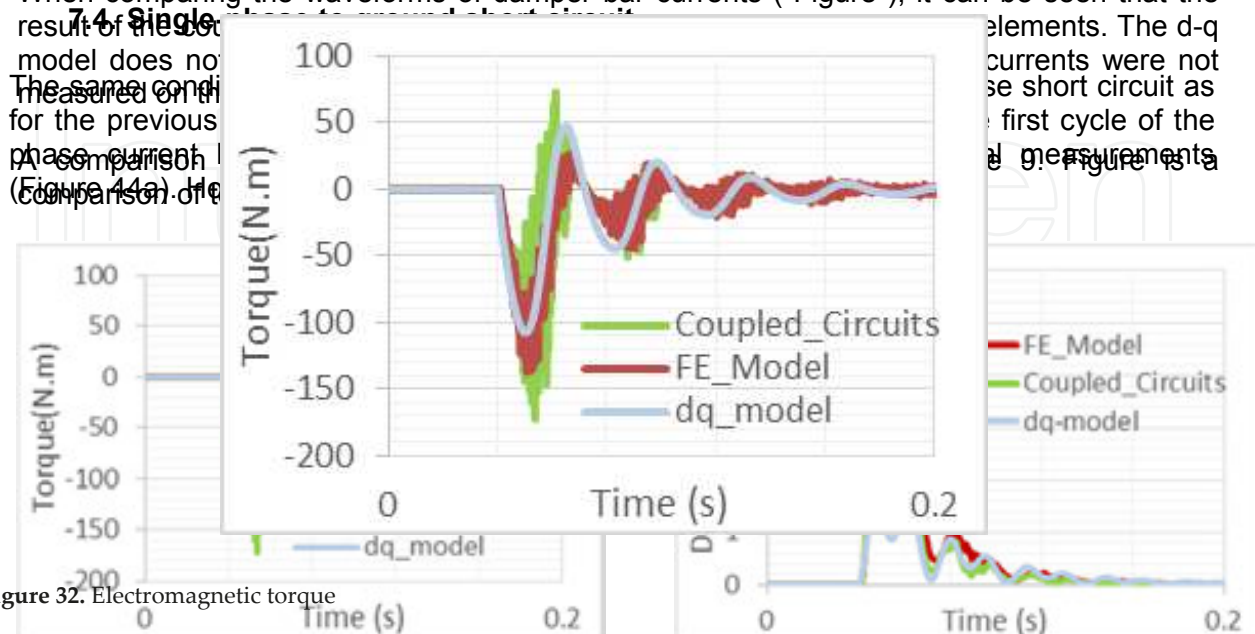
Figure 32. Electromagnetic torque

Figure 9: Electromagnetic torque

Figure 33: Total copper losses of damper circuit

As the d-q model neglects all voltage and slotting harmonics, the high-frequency torque oscillations are filtered (Figure 9). The torque calculation methods of the two other models (FE and coupled circuit) lead to similar waveforms. It suggests that the electromagnetic torque peaks at 180 Nm (6.4 pu) compared to 110 Nm for the d-q model. One can also conclude that the assumptions used in the coupled-circuit model are valid. The finite

As the d-q model neglects all voltage and slotting harmonics, the high-frequency torque oscillations are filtered (Figure 9). The torque calculation methods of the two other models (FE and coupled circuit) lead to similar waveforms. It suggests that the electromagnetic torque peaks at 180 Nm (6.4 pu) compared to 110 Nm for the d-q model. One can also conclude that the assumptions used in the coupled-circuit model are valid. The finite element method takes account of the skin effect in the bars. This explains that the damper losses are near twice larger than the other models' estimations (Figure).

7.2. Two-phase short circuit without neutral connection at full voltage

The same conditions are used for the simulation of the sudden two-phase short circuit as for the previous section on the sudden three-phase short circuit.

From Figure to Figure , the phase and field currents are compared. A similar error can be seen on the evaluation of the first current peak. The possible advantage of a finite element simulation in obtaining these current waveforms is not entirely clear.
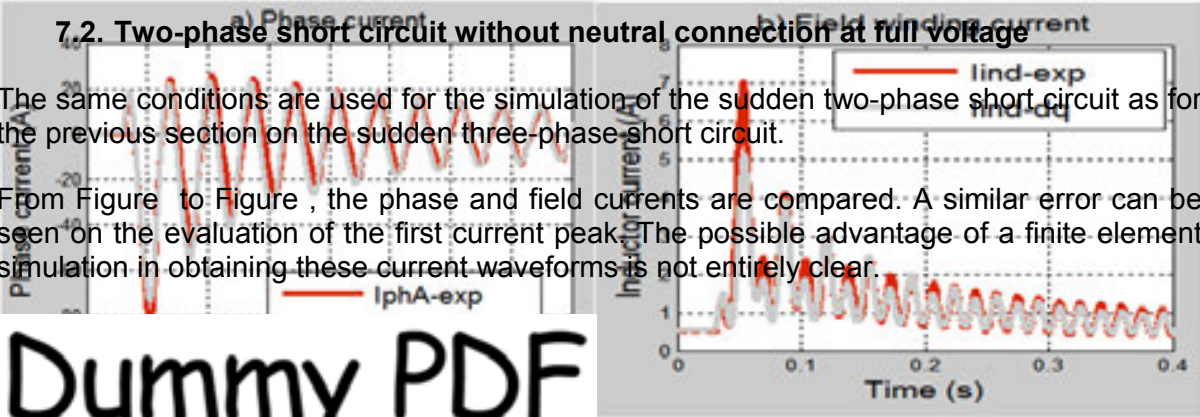
Figure 34: Two-phase short circuit; d-q model with saturation vs experiment
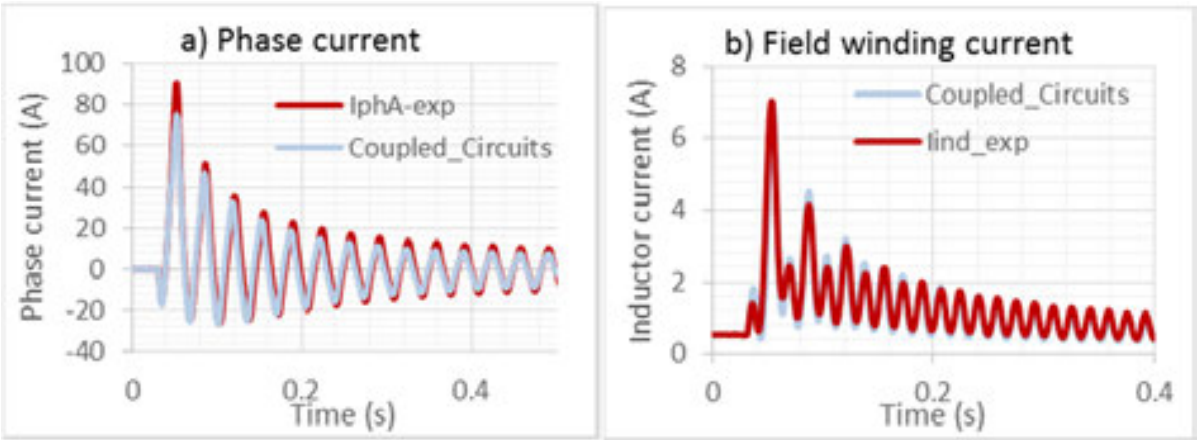
Figure 35: Two-phase short circuit; coupled circuit model vs experiment
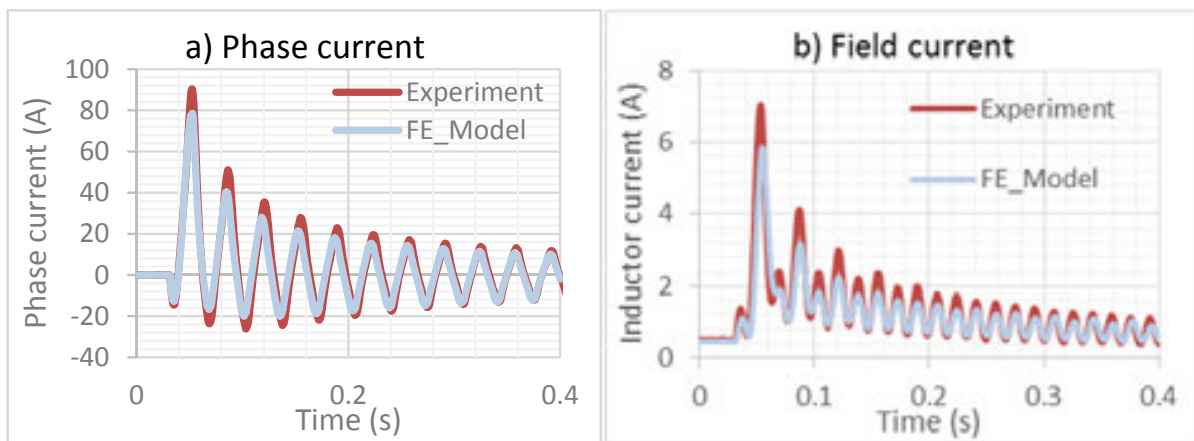
Figure 36: Two-phase short circuit; finite element model vs experiment

Comparing the waveforms of the damper bar currents shows that the coupled-circuit model provides results very close to the finite element model (Figure 37).
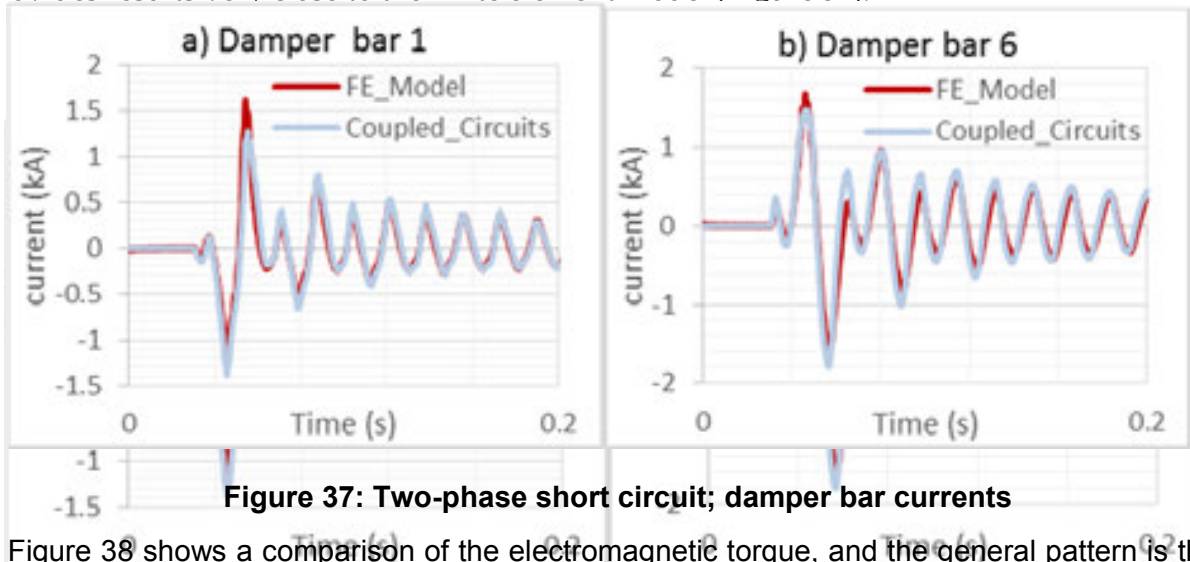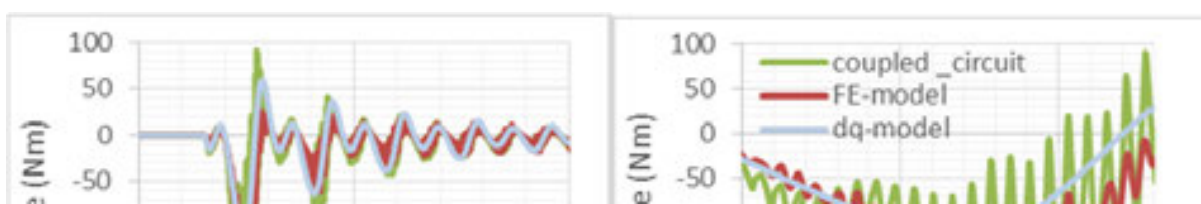

Figure 37: Two-phase short circuit; damper bar currents

Figure 38 shows a comparison of the electromagnetic torque, and the general pattern is the same for all simulation methods. The two first periods are detailed on the second figure. The torque oscillations are slower with the finite element than with the coupled-circuit model. However, the waveforms of the finite element and coupled-circuit models are very similar after several periods when the current is lower (Figure 39). Some local magnetic saturation could explain this attenuation of torque oscillations, but the numerical methods used may be also involved.

Figure 40 presents the damper circuit losses. The highest peak value (7 kW) is obtained with the finite element method, during the first period, according to the skin effect. The dq model underestimates these losses, but the differences are reduced afterward.

We conclude that a simple magnetic saturation modelling method provides valid current waveforms, and the skin effect has little influence on the current waveforms. The largest differences between the models are related to the electromagnetic torque and the damper bar losses.

However, the waveforms of the finite element and coupled-circuit models are very similar after several periods when the current is lower (Figure 39). Some local magnetic saturation could explain this attenuation of torque oscillations, but the numerical methods used may be also involved.

Figure 40 presents the damper circuit losses. The highest peak value (7 kW) is obtained with the finite element method, during the first period, according to the skin effect. The d-q model underestimates these losses, but the differences are reduced afterward.

We conclude that a simple magnetic saturation modelling method provides valid current waveforms, and the skin effect has little influence on the current waveforms. The largest differences between the models are related to the electromagnetic torque and the damper bar losses.
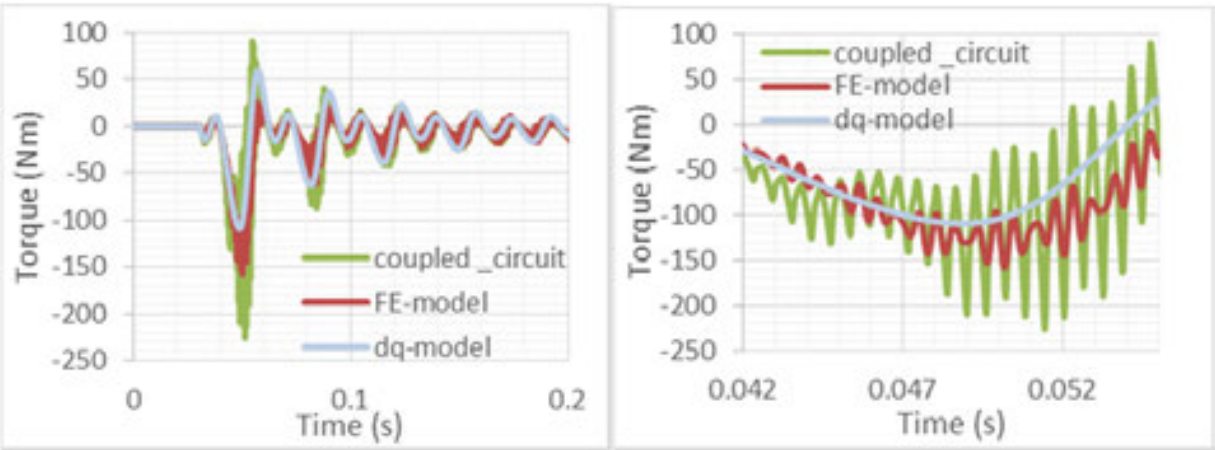

Figure 10: Electromagnetic torque (general pattern and detail 1)

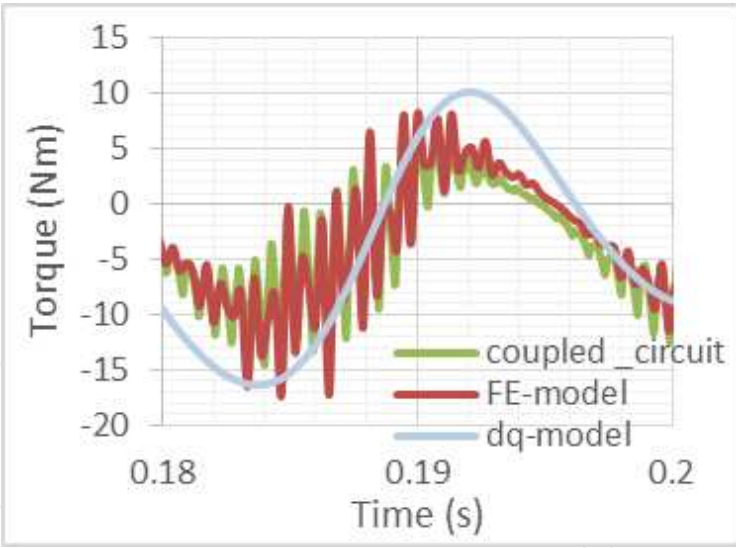Figure 38. Electromagnetic torque (general pattern and detail 1)

Figure 39. Torque (detail 2)

7.3. Two-phase short circuit with neutral–ground connection

The neutral connection to the ground changes the current waveform because the harmonics multiple of three have high amplitudes in the phase emf voltage. It should be noted that the Matlab d-q model cannot simulate short circuits with neutral connection because the emf harmonics and homopolar current are neglected.
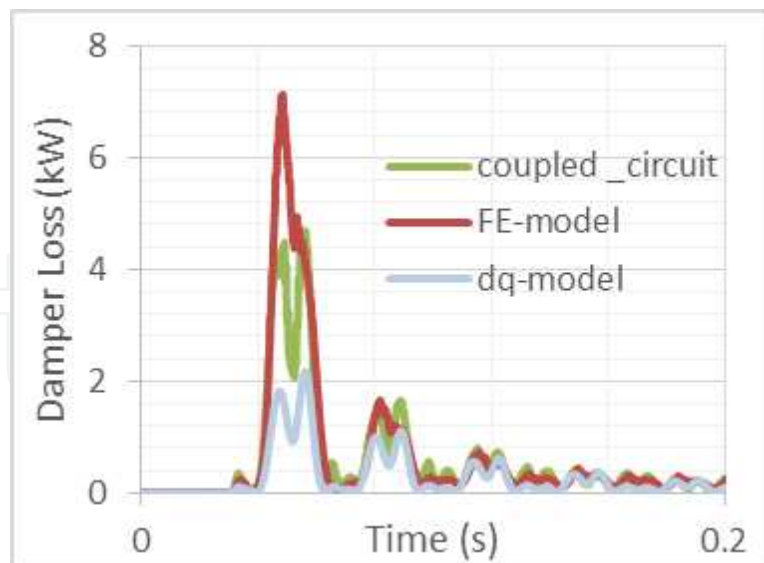
Figure 40. Copper losses of damper circuit

Figures 41 and 42 compare the two-phase short-circuit responses at low field current (0.22 A–0.44 pu). The results are better with the finite element model (Figure 42) than the coupled-circuit model (Figure 41). Explanations are provided in section 7.1.

Figure 43 shows that the damper current waveforms calculated by the finite element model are close to the ones provided by the coupled-circuit model. Again, the coupled-circuit model underestimates these currents.
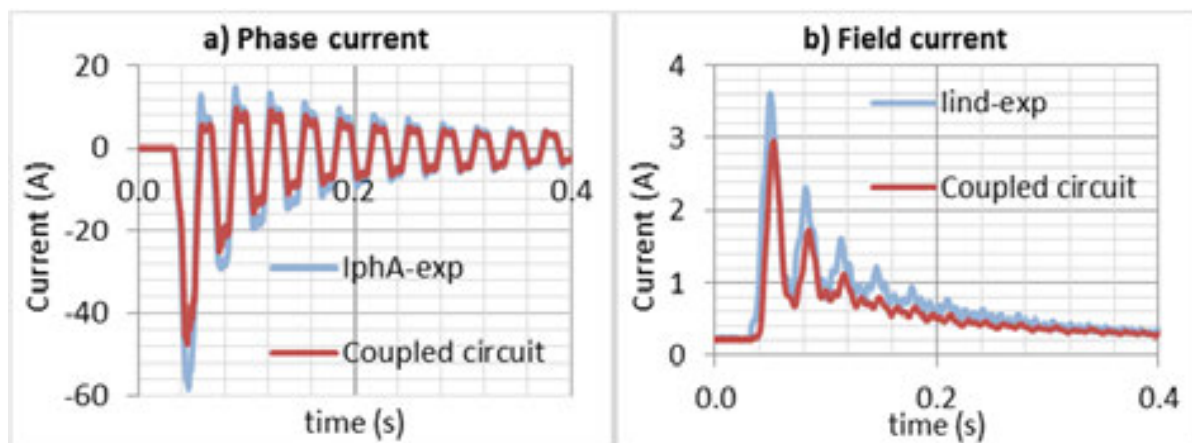

Figure 11: Two-phase short circuit; coupled circuit model vs experiment

Figure 41. Two-phase short circuit; coupled circuit model vs experiment

7.4. Single-phase to ground short circuit

The same conditions are used for the simulation of the sudden single-phase short-circuit as for the previous section. In this case, there is a difference of 20 A on the first cycle of the phase
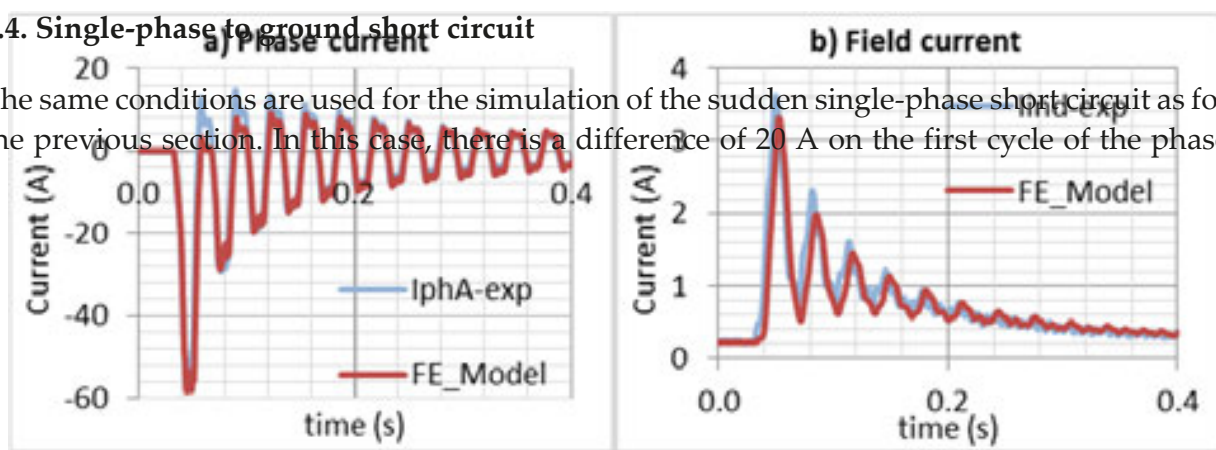
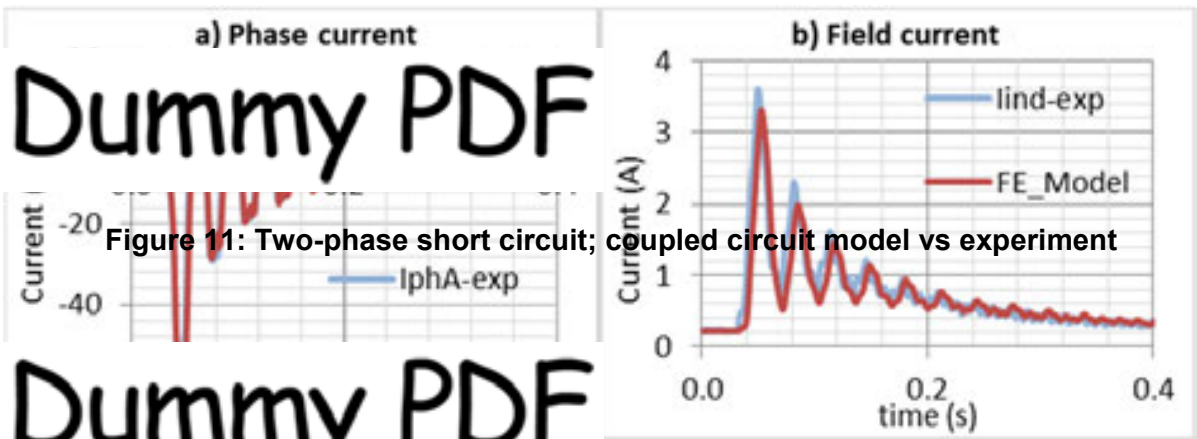Figure 11: Two-phase short circuit; coupled circuit model vs experiment

Figure 42. Two-phase short circuit; finite element model vs experiment

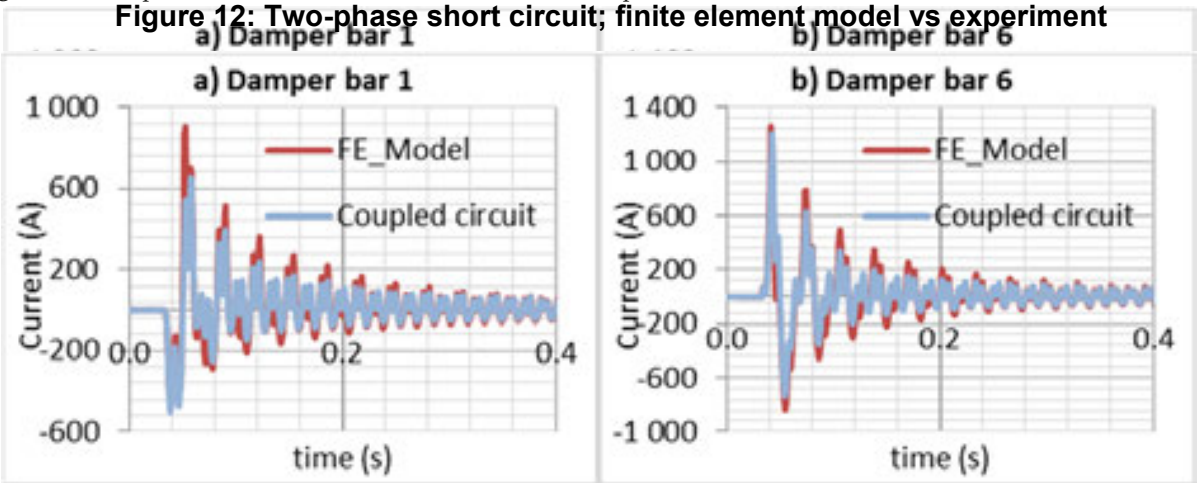Figure 12: Two-phase short circuit; finite element model vs experiment

Figure 43. Two-phase short circuit; damper bar currents

Figure 13: Two-phase short circuit; damper bar currents

7.4. Single-phase to ground short circuit

The same conditions are used for the simulation of the sudden single-phase short circuit as for the previous section. In this case, there is a difference of 20 A on the first cycle of the phase current between the coupled-circuit model and the experimental measurements (Figure 44a). However, the field current waveforms are close (Figure 44b).

The results of FE model showed a good agreement with the experimental phase current waveform (Figure 45a). More differences are observed on the field current waveform (Figure 45b). This phenomenon may be related to the discretization chosen during simulation.
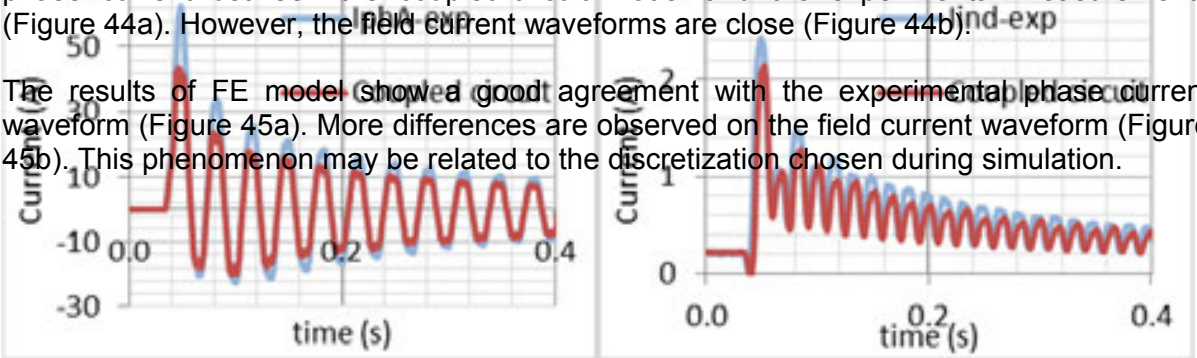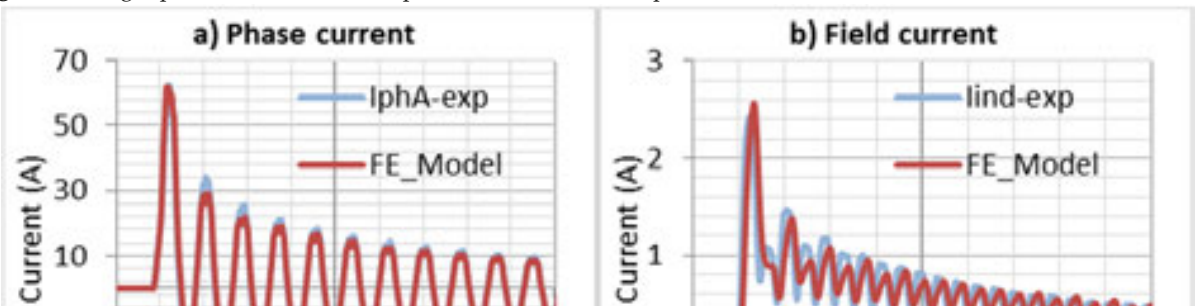

Figure 44. Single-phase short circuit; coupled circuit model vs experiment

Figure 44: Single-phase short circuit; coupled circuit model vs experiment

The results of FE model show a good agreement with the experimental phase current waveform (Figure 45a). The field current response of the FE model appears to be filtered (Figure 45b). This phenomenon may be related to the discretization chosen during simulation.
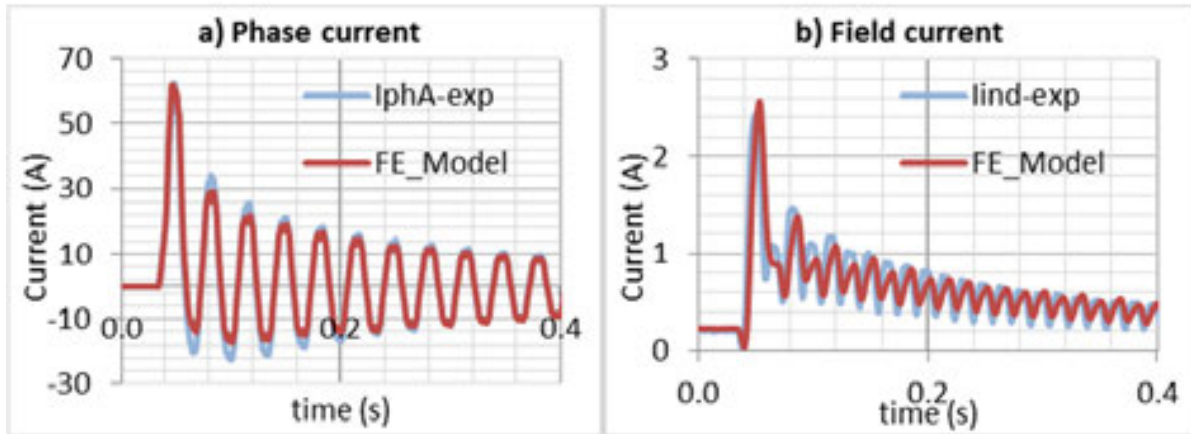

Figure 45. Single-phase short circuit; finite element model vs experiment

8   Conclusion

We have presented three electrical machine models:

- The d-q model is widely used for protection, control, and stability studies. This model is available from Matlab-Simulink library. One way to identify the d-q model parameters without short-circuit tests is to carry out a test of standstill frequency response (SSFR). This test may be performed using an experimental setup or as a finite element method in complex. This model is fast and represents accurately the waveforms of the currents in the stator and the field winding.

- The coupled-circuit model is a high-order circuit model that considers all space harmonics in the machine and all winding configurations. We presented a method that uses a 2D finite element method to compute the magnetic couplings and evaluate discrete inductance variations according to the rotor position. This model is easy to implement in Matlab-Simulink. It has the advantage of combining the precision of the finite element spatial representation for the magnetic couplings, with efficient variable time-step solvers. It is a bit slower than the d-q model, but gives better accuracy on the phase and field signal waveforms. In addition, this model can estimate the currents in other circuits, such as the damper bars. This improves the estimation of transient torque and provides results closer to the finite element method.

- The finite element model using a magnetodynamic solver with the rotor movement is the more general approach to obtain local magnetic data in various parts of the machine. This analysis requires a perfect knowledge of the machine's geometry and material properties. The main drawback of this method is the simulation time. This model is the most accurate with regard to the local magnetic saturations and the damper bar losses with the skin effect. It also gives the best estimation of magnetic losses.

We showed that all three models are efficient to estimate the transient response of an electrical generator. Comparisons were made with a laboratory generator by performing various types of short circuit at various excitation levels. It was shown that the magnetic saturation must be taken into account for a generator in normal operation.

analysis requires a perfect knowledge of the machine's geometry and material properties. The main drawback of this method is the simulation time. This model is the most accurate with regard to the local magnetic saturations and the damper bar losses with the skin effect. It also gives the best estimation of magnetic losses.

We showed that all three models are efficient to estimate the transient response of an electrical generator. Comparisons were made with a laboratory generator by performing various types of short circuit at various excitation levels. It was shown that the magnetic saturation must be taken into account for a generator in normal operation.

Acknowledgements

Author details

Jérôme Cros[*], Stéphanie Rakotovololona, Maxim Bergeron, Jessy Mathault, Bouali Rouached, Mathieu Kirouac and Philippe Viarouge

*Address all correspondence to: cros@gel.ulaval.ca

LEEPCI, Laval University, Quebec, Qc, Canada

References

[1] I. Boldea, Synchronous Generators, 1st ed. CRC Press, USA, 2005.

[2] D. Aguglia, P. Viarouge, R. Wamkeue, J. Cros, "Optimal Selection of Drive Components for Doubly-Fed Induction Generator Based Wind Turbines," InTech, ISBN 978-953-307-221-0, 4 April 2011. http://www.intechopen.com/books/wind-turbines

[3] D. Aguglia, P. Viarouge, R. Wamkeue, J. Cros, Determination of fault operation dynamical constraints for the design of wind turbine DFIG drives. Mathematics and Computers in Simulation, vol. 81, no. 2, p. 252–262, 2010.

[4] "IEEE Guide for Synchronous Generator Modeling Practices and Applications in Power System Stability Analyses," IEEE Std 1110-2002 Revis. IEEE Std 1110–1991, pp. 0_1–72, 2003.

[5] "Approved IEEE Recommended Practice for Excitation Systems for Power Stability Studies (Superseded by 421.5-2005)," IEEE Std P4215D15, 2005.

[6]   "IEEE Guide for Test Procedures for Synchronous Machines Part I Acceptance and Performance Testing Part II Test Procedures and Parameter Determination for Dynamic Analysis." 2011.

[7]   P. Kundur, Power system stability and control. New York: McGraw-hill, 1994.

[8]   T.A. Lipo, Analysis of Synchronous Machines, 2nd ed. CRC Press Taylor & Francis Group, USA, 2012

[9]   E. Deng, N.A.O. Demerdash, A coupled finite-element state-space approach for synchronous generators. I. Model development. IEEE Transactions on Aerospace and Electronic Systems, vol. 32, no. 2. pp. 775–784, 1996.

[10] I. Kamwa, P. Viarouge, H. Le-Huy, E.J. Dickinson, A frequency-domain maximum likelihood estimation of synchronous machine high-order models using SSFR test data. IEEE-Energy Conversion, vol. 7, no. 3, pp. 525–536, 1992.

[11] M. Ghomi and Y. N. Sarem, Review of synchronous generator parameters estimation and model identification. 42nd International Universities Power Engineering Conference, 2007. UPEC 2007, pp. 228–235, 2007.

[12] JPA. Bastos, N. Sadowski, Electromagnetic modeling by finite element methods, CRC press, USA, 1, avril 2003

[13] I. Kamwa, P. Viarouge, H. Le-Huy, E.J. Dickinson, Three-transfer-function approach for building phenomenological models of synchronous machines. IEE Proceedings-Generation, Transmission and Distribution, vol.141, no. 2, pp. 89–98, 1994.

[14] "IEEE Standard Procedures for Obtaining Synchronous Machine Parameters by Standstill Frequency Response Testing (Supplement to ANSI/IEEE Std 115-1983, IEEE Guide: Test Procedures for Synchronous Machines)," IEEE Std 115A-1987, p. 0_1, 1987.

[15] Flux2D Cedrat, user guides and technical paper on synchronous motor, 2015, http://www.cedrat.com/

[16] X. Luo, Y. Liao, H. Toliyat, A. El-Antably, T.A. Lipo, Multiple coupled circuit modeling of induction machines. Transaction on IEEE Industry Applications Society, vol 31, no2, pp. 311–318, 1995.

[17] A. Tessarolo, Accurate computation of multiphase synchronous machine inductances based on winding function theory. IEEE Transactions on Energy Conversion, vol. 27, no. 4, pp. 895–904, 2012

[18] J. Mathault, M. Bergeron, S. Rakotovololona, J. Cros, P. Viarouge, "Influence of discrete inductance curves on the simulation of a round rotor generator using coupled circuit method", Electrimacs 2014, 2014 May 19–22, Valencia (ESP).

[19] M. Benecke, G. Griepentrog, A. Lindemann, Skin effect in squirrel cage rotor bars and its consideration in non-steady state operation of induction machines, PIERS online, vol. 7, p. 5, 2011.

[20] T.W. Nehl, F.A. Fouad, N.A. Demerdash, Determination of saturated values of rotating machinery incremental and apparent inductances by an energy perturbation method. IEEE Transactions on Power Apparatus and Systems, vol. PAS-101, no. 12, pp. 4441–4451, 1982.

[21] J.E. Brown, K.P. Kovacs, P. Vas, A method of including the effects of main flux path saturation in the generalized equations of AC machines. IEEE Transactions on Power Apparatus and Systems, vol. 1, pp. 96–103, 1983.

[22] S.A. Tahan, I. Kamwa, A two-factor saturation model for synchronous machines with multiple rotor circuits. IEEE Transactions on Energy Conversion, vol. 10, no. 4, pp. 609–616, 1995.